Magnetic moments of the octet, decuplet, low-lying charm, and low-lying bottom baryons in a nuclear medium

K. Tsushima[*]

Laboratório de Física Teórica e Computacional-LFTC, Universidade Cidade de São Paulo and Universidade Cruzeiro do Sul, 01506-000, São Paulo, SP, Brazil
[*]E-mail: kazuo.tsushima@gmail.com

....

We study the magnetic moments of the octet, decuplet, low-lying charm, and low-lying bottom baryons with nonzero light quarks in symmetric nuclear matter using the quark–meson coupling (QMC) model, which satisfies the constraint for the allowed maximum change (swelling) of the in-medium nucleon size derived from the y-scaling data for ^{3}He(e, $e^{'}$) and ^{56}Fe(e, $e^{'}$). This is the first study to estimate the in-medium magnetic moments of the low-lying charm and bottom baryons with nonzero light quarks. The present QMC model also satisfies the expected allowed maximum enhancement of the nucleon magnetic moments in nuclear matter. Moreover, it has been proven that the calculated in-medium to free proton electromagnetic form factor (EMFF) ratios calculated within the QMC model reproduce well the proton EMFF super ratio extracted from ^{4}He($\vec{e}$, $e'\vec{p}$)^{3}H at Jefferson Laboratory. The medium modifications of the magnetic moments are estimated by evaluating the in-medium to free space baryon magnetic moment ratios to compensate the MIT bag deficiency to describe the free space octet baryon magnetic moments, where ratios are often measured directly in experiments even without knowing the absolute values, such as the free and bound proton electromagnetic form factors, as well as the European Muon Collaboration effect to extract the structure function F_2 ratio of the bound to free nucleons by the corresponding cross section ratio. We also present the results calculated with the different current quark mass values for the strange and bottom quarks to see the possible impact. Furthermore, for practical use we give the explicit density-dependent parametrizations for the vector potentials of the baryons and light-(u, d) quarks, as well as for the effective masses of the baryons treated in this study, and of the mesons ω, ρ, K, K^*, η, η', D, D^*, B, and B^*.

....

Subject Index   D32, D33

1. Introduction

Studying the properties of hadrons containing both the heavy quarks (charm (c) and bottom (b)) and the isodoublet light quarks (up (u) and down (d)) is particularly interesting, since the heavy quarks can be regarded as static color/gluon sources, while the isodoublet light quarks surrounding them can be regarded as interacting strongly with other hadrons. (Hereafter, we will simply denote the isodoublet light quarks u and d as light quarks, but not the strange quark s, unless otherwise stated.) This gives an alternative picture for the structure of heavy hadrons additional to that of the hadrons composed of purely light quarks. In heavy hadrons with light quarks, the light quarks contribute to their masses by dynamical symmetry breaking. Thus, when the heavy hadrons with nonzero light quarks are produced in nuclei, e.g. in the future antiProton ANnihilations at DArmstadt (PANDA) experiment, we can advance our

understanding of hadron structure [1]. The physics of PANDA aims explicitly to produce the heavy hadrons in nuclei among the other physics issues. Of course, to study the in-medium properties of hadrons with strange (s) quarks, such as (strange) hyperons, is also very interesting and important in connection with the strange hypernuclei, and the "hyperon puzzle" in neutron star structure.

In astrophysical laboratories such as neutron stars and compact stars, as well as in the dense nuclear medium produced in heavy ion collisions, the effects of the strong magnetic field on the hadron properties have been studied [2–17]. Furthermore, the effects of the baryon (anomalous) magnetic moments on (proto-)neutron star structure under very strong magnetic fields were investigated in Refs. [6,11,15,16]. Moreover, the effects of the charm quark in a dense medium, namely the stability of a charm star, was studied in Refs. [18–20].

In this study we focus on the modifications of baryon magnetic moments in a nuclear medium of the octet, decuplet, the low-lying charm, and the low-lying bottom baryons with nonzero light quarks. Through this, we can study the in-medium electromagnetic interactions of the light and heavy baryons, the differences in the medium modifications, and the roles of the light and heavy quarks in a nuclear medium.

We studied in Ref. [21] the strong interaction properties for the octet, low-lying charm, and low-lying bottom baryons with nonzero light quarks in symmetric nuclear matter by the quark–meson coupling (QMC) model invented by Guichon [22]. In this study, we extend further to include the decuplet baryons, and proceed to study the modifications of the magnetic moments in a nuclear medium that have potential impacts on studies of neutron star and magnetar structure. In particular, the Δ baryon properties in a nuclear medium have garnered renewed interest [23–32].

The QMC model has been successfully applied in various studies, e.g. for the properties of finite (hyper)nuclei [33–42], in-medium hadron properties in medium [43–49], nuclear reactions [50–58], and neutron star structure [59–63]. (See Refs. [64–66] for reviews.) It should be emphasized that the $^{15}_{\Xi}$C hypernucleus single-particle energies predicted by the QMC model [39,67] were indeed observed very closely in experiments [68]. This may give some confidence in the treatment of the strange quark sector in the QMC model to be explained below.

Self-consistent exchange of the Lorentz-scalar-isoscalar σ-, Lorentz-vector-isoscalar ω-, and Lorentz-vector-isovector ρ-meson fields, coupled directly to confined, relativistically moving, light u and d quarks, is the key mechanism of the QMC model. This mechanism, though simple, is known to achieve novel saturation properties of nuclear matter: saturation is achieved due to the quark structure of the nucleon and quark dynamics. All the relevant coupling constants between the light quarks and the σ-, ω-, and ρ-meson fields in any hadrons can be treated the same as those in the nucleon, once the coupling constants are determined/constrained by the fit to the nuclear matter saturation constraints.

The physics behind the simple picture of the QMC model is associated with dynamical symmetry breaking, although the usual QMC model, such as the present one, does not have explicit chiral symmetry due to the lack of a pion (Goldstone boson) field in the model. (See Refs. [69,70] for the chiral quark–meson coupling (CQMC) model, which explicitly incorporates the pion field using the cloudy bag model instead of the MIT bag model, to be consistent with chiral symmetry.) Namely, the light-quark condensates are expected to reduce the magnitude faster than those of the strange and heavier quarks as nuclear density increases, and this is supported by: (i) studies of the in-medium strange and light quark condensates in connection with

the ϕ-meson mass shift in nuclear matter in the quantum chromodynamics (QCD) sum rule approach [71,72] (see also P. Gubler, private communication, August 2021), (ii) studies based on the NJL model [73,74] for the strange and light quark condensates in medium, and (iii) the result that the heavy quark condensates are proportional to the gluon condensate that is obtained by the operator product expansion [75] and also by a world-line effective action-based study [76], together with the model-independent result that the magnitude of gluon condensate at the nuclear matter saturation density decreases by only about 5 QCD trace anomaly and Hellman–Feynman theorem [77]. The light quark condensates are associated with dynamical chiral symmetry breaking and partial restoration of chiral symmetry in the nuclear medium, where the latter is related to the reduction of the light quark condensates. Although the QMC model Lagrangian does not have chiral symmetry, the model incorporates the expected facts of the density dependence of the in-medium quark condensates phenomenologically. That is, the model approximates that the σ-, ω-, and ρ-meson fields couple directly only to the light quarks, but not to the strange or heavier quarks. Although one can consider the couplings of strange quark with the ϕ-meson field and some other types of Lorentz scalar-meson fields, these would introduce unconstrained coupling constants which cannot be determined/constrained by the nuclear matter saturation properties, where the nuclear matter saturation properties are the basic properties for calibrating any reasonable nuclear matter model.

As mentioned already, studying the in-medium properties of heavy baryons with nonzero light quarks is very important to understand dynamical symmetry breaking, its partial restoration, and the roles of the light quarks in medium. These phenomena can provide us with additional information on the origin of (dynamical) masses of hadrons and "normal" (not "dark") matter, which we can observe directly in our universe. Because of the importance, many studies have been undertaken for heavy baryon hypernuclei as well as the properties of heavy baryons with nonzero light quarks in a nuclear medium [40–42,49,78–99].

In effective models such as the present one, the (current) quark mass values do not have a direct connection with QCD, but we may regard the quark mass value effect as a model parameter dependence. We therefore also present the results calculated with different values of the current quark masses for the strange and bottom quarks in this study. Although the magnetic moments of the octet [100–102] and decuplet [103] baryons in medium were studied, there are currently no studies for the low-lying charm or bottom baryons with nonzero light quarks in a nuclear medium, while some studies in free space have been performed with symmetry-based quark models [104–106], the MIT bag model [107–110], QCD sum rules [111,112], a relativistic three-quark model [113], a nonrelativistic hyper central model [114], an independent-quark model based on the Dirac equation [115], and a relativistic potential model [116].

As for the in-medium modification of the bound nucleon size, or the bound nucleon electromagnetic form factors (EMFFs) which are directly associated with the present study, the constraint on the allowed maximum change (swelling) of the bound nucleon size was derived by the y-scaling data for ^{3}He(e, e') [117] and ^{56}Fe(e, e') [118]. It was concluded that the allowed maximum increase of the bound nucleon size is 3%–6% in ^{3}He and 2%–3% in ^{56}Fe. More precise analysis was performed by McKeown, and the upper limit of 3.6% in ^{3}He was obtained [119]. Larger upper limit values may possibly be obtained by different methods. In Ref. [120] the relative change of the proton charge radius of 13% $\pm$ 4% in a heavy nucleus was suggested, based on analysis of the longitudinal Coulomb response function (Coulomb sum rule) using the effective momentum approximation, where the quenching of the longitudinal response

function was reinterpreted assuming the dipole expression for the proton charge form factor. However, the derived value seems to be more indirect than that obtained by the *y*-scaling data analysis.

The bound nucleon size (charge and magnetic radii) has been discussed in the past in connection with the predictions of the bound nucleon EMFFs in the QMC [121,122] and CQMC models [69]. In Ref. [122] it was stated that the 10% decrease of the bag constant at the normal nuclear matter density ρ_0 (=0.15 fm^{-3}) is already quite large, and this would severely reduce the bound nucleon EMFFs. Using the average baryon density estimated by the QMC model, $\langle\rho_B(^3\mathrm{He})\rangle \simeq 0.35\rho_0$ and $\langle\rho_B(^{56}\mathrm{Fe})\rangle \simeq 0.71\rho_0$, the *y*-scaling-based results lead to allowed maximum change (swelling) of the nucleon size at ρ_0 of 8.5%–17.1% and 4.2%–8.5% respectively. Since the MIT bag model for both the matter (charge) radius and the magnetic moment of the proton are proportional to the bag radius, neither the bag radius nor the nucleon magnetic moment at ρ_0 can be enhanced by more than 17.1% if one takes the *y*-scaling result properly. Although the range 4.2%–8.2% derived from the ^{56}Fe data is expected to be more appropriate to extrapolate to the normal nuclear matter density ρ_0, we allow the larger range in the discussion. There have been studies of the in-medium octet baryon magnetic moments [100] and their impact on neutron stars under a strong magnetic field [11], and the authors reported about a 25% enhancement of the nucleon magnetic moment, and about a 20% increase of the nucleon bag radius at a density of 0.17 fm^{-3} ($1.133\rho_0 = 1.133 \times 0.15$ fm^{-3}). The results seem to give too large an enhancement, which originates from the density-dependent bag constant using the modified quark–meson coupling (MQMC) model. In this study we use the standard QMC model, and indeed the results will turn out to satisfy even the tighter *y*-scaling data constraint. Thus, the present results are expected to be constrained by the allowed in-medium modifications of the octet baryon magnetic moments, as well as for those of the decuplet and low-lying charm and bottom baryons with nonzero light quarks.

Although it is known that the MIT bag model has a deficiency in producing the magnitude of the free-space octet baryon magnetic moments, we can focus on the in-medium to free space ratios, as many experiments directly measure ratios to extract meaningful physical quantities, such as to extract the free proton [123,124] or bound proton [125,127,128] EMFF ratios by simultaneously measuring the transverse (P_t) and longitudinal (P_l) recoil proton polarization to extract the proton electric (G_E^p) over magnetic (G_M^p) form factor ratio $G_\mathrm{E}^p/G_\mathrm{M}^p$. Indeed, the super ratio $[G_\mathrm{E}^p/G_\mathrm{M}^p(^4\mathrm{He})]/[G_\mathrm{E}^p/G_\mathrm{M}^p(^1\mathrm{H})]$ calculated using the in-medium to free EMFF "ratios" predicted by the QMC model reproduce the data well, as shown in Refs. [125–127]. Note that the meson cloud contributions for the total medium modifications of EMFFs are of the order of a few tens percent, namely 0.2%∼0.3% for total modifications of about 10%. Furthermore, the relativistic kinematic factors are canceled out in the EMFF ratios calculated with the QMC model. Because the in-medium modifications apply directly for the light quarks in the QMC model and the reproduced data are for a proton composed of purely light quarks, as far as the effects of light quarks are concerned we may have some confidence in the in-medium to free EMFF ratios for the strange and heavy baryons, where the light quark medium modifications are mainly responsible for the medium modifications of these baryons. Recall also the successful predictions for the $^{15}_\Xi\mathrm{C}$ hypernucleus single-particle energies associated with the strange quark sector.

Furthermore, in Ref. [123] it is stated that for the method of measuring the ratio, "Neither the beam polarization nor the polarimeter analyzing power needs to be known, which

results in small systematic uncertainties." The examples for the experiments mentioned above clearly demonstrate the usefulness of measuring/calculating ratios of physical quantities. Another example is to extract the structure function (F_2) ratio of the bound to free nucleons, [$F_2^{\text{bound nucleon}}/F_2^{\text{free nucleon}}$] by measuring the corresponding cross section ratio (see, e.g., Ref. [129,130]), known as the "EMC" effect (ratios) [131].

Concerning the magnetic moments of heavy baryons with c and/or b quark(s), some ambiguities arise in constructing the flavor–spin wave functions [106]. These are associated with the so-called "quark order," originating from the fact that the spin, isospin, SU(3) flavor symmetry and the Pauli principle cannot help much. The possible different quark orders in the flavor–spin wave functions yield different results for the calculated magnetic moments. This concerns the $\Xi_{c,b}$ baryons in the present study. For these $\Xi_{c,b}$ baryons, the two lightest quarks (u and s) or (d and s) are taken as the first two quark antisymmetric pairs, denoted as [u, s] or [d, s], in the wave functions [132], and thus the magnetic moments of $\Xi_{c,b}$ are given by $\mu_{c,b}$ [106,108] and are nearly the same as those of the $\Lambda_{c,b}$. Thus, the free as well as the in-medium magnetic moments of the $\Xi_{c,b}$ are almost the same as those of the $\Lambda_{c,b}$ baryons, as will be shown explicitly later. Thus, although some issues exist for the quark order as discussed in Ref. [106], we may assume the natural quark order as realized for the octet baryon sector, and study the magnetic moments and the transition magnetic moments of the octet, decuplet, low-lying charm, and low-lying bottom baryons with nonzero light quarks in symmetric nuclear matter. Note that the "1–2 quark order" is supported in Ref. [106] as the best quark ordering for flavor-degenerate baryons for the masses. Furthermore, we discuss possible ambiguities originating from the MIT bag model artifact for the transition magnetic moments. This is the first study to estimate the in-medium magnetic moments of the low-lying charm and bottom baryons with nonzero light quarks.

As an important side remark, we would like to emphasize that the explicit density-dependent parametrizations are given for the vector potentials of the baryons and light (u, d) quarks, as well as for the effective masses (Lorentz-scalar-isoscalar mean field potentials) of the low-lying baryons treated in this study, and of the ω, ρ, K, K^*, η, η', D, D^*, B, and B^* mesons for practical use.

2. The QMC model

In this section we outline the QMC model following Refs. [64,65]. Since the Hartree–Fock approximation in the QMC model gives very similar results to those of the Hartree approximation [133], we use the Hartree approximation to be consistent with Ref. [21]. (See Ref. [62] for the Hartree–Fock approximation in the QMC model applied for studying the neutron star structure with hyperons.)

Furthermore, the one-gluon-exchange-based color–magnetic interaction between the quarks, which enhances the in-medium mass splittings between the Σ and Λ baryons [39] as well as the N and Δ baryons [29], playing an important role in studies of hypernuclei and neutron star structure, is not included in this study.

In a practical aspect, we would like to emphasize that the explicit density-dependent parametrizations for the Lorentz-vector potentials of the baryons, as well as for the effective masses (Lorentz-scalar-isoscalar potentials) of the low-lying baryons and mesons except for the pion, will be given in this section.

2.1   *Nuclear matter*

Using the Born–Oppenheimer approximation, a relativistic effective Lagrangian density for a "hypernucleus" in the QMC model may be given by the following [38,42,64,65] (to consider the nuclear matter limit, we call the following configuration a "hypernucleus" using the terminology "hyperon (Y)" for each baryon indicated in Eq. (3)):

$$\mathcal{L}_{\mathrm{QMC}}^{HY} = \mathcal{L}_{\mathrm{QMC}}^{N} + \mathcal{L}_{\mathrm{QMC}}^{Y}, \tag{1}$$

$$\mathcal{L}_{\mathrm{QMC}}^{N} = \overline{\psi}_N(\vec{r})\left[i\gamma\cdot\partial - m_N^*(\sigma) - \left(g_\omega\omega(\vec{r}) + g_\rho\frac{\tau_3^N}{2}b(\vec{r}) + \frac{e}{2}(1+\tau_3^N)A^0(\vec{r})\right)\gamma_0\right]\psi_N(\vec{r})$$

$$- \frac{1}{2}\left[(\nabla\sigma(\vec{r}))^2 + m_\sigma^2\sigma(\vec{r})^2\right] + \frac{1}{2}\left[(\nabla\omega(\vec{r}))^2 + m_\omega^2\omega(\vec{r})^2\right]$$

$$+ \frac{1}{2}\left[(\nabla b(\vec{r}))^2 + m_\rho^2 b(\vec{r})^2\right] + \frac{1}{2}(\nabla A^0(\vec{r}))^2, \tag{2}$$

$$\mathcal{L}_{\mathrm{QMC}}^{Y} = \overline{\psi}_Y(\vec{r})\left[i\gamma\cdot\partial - m_Y^*(\sigma) - \left(g_\omega^Y\omega(\vec{r}) + g_\rho^Y I_3^Y b(\vec{r}) + eQ_Y A^0(\vec{r})\right)\gamma_0\right]\psi_Y(\vec{r})$$

$$\left(Y = \Lambda,\ \Sigma^{0,\pm},\ \Xi^{0,-},\ \Delta^{0,\pm,++},\ \Sigma^{*0,\pm},\ \Xi^{*0,-},\ \Lambda_c^+,\ \Sigma_c^{0,+,++},\ \Xi_c^{0,+},\ \Lambda_b^0,\ \Sigma_b^{0,\pm},\ \Xi_b^{0,-}\right), \tag{3}$$

where the quasi-particles moving in single-particle orbits are three-quark clusters with the quantum numbers of a nucleon, a Δ baryon, a strange, a charm, or a bottom "hyperon" when expanded to the same order in velocity [33,34,38,40,42,49]. In the above, $\psi_N(\vec{r})$ [$\psi_Y(\vec{r})$] is the nucleon [Δ baryon, hyperon (strange, charm, or bottom baryon)] field. The mean-meson fields represented by σ, ω, and b are the Lorentz-scalar-isoscalar, Lorentz-vector-isoscalar, and third component of the Lorentz-vector-isovector fields, respectively, while A^0 is the Coulomb field. Hereafter, the quantities in medium will be denoted with an asterisk superscript. Note that in the Lagrangian density of Eq. (3), the phenomenologically introduced effective Pauli potentials, which also contain the channel-coupling effects at the baryon level for the Λ, Σ, and Ξ [38], are not written explicitly. The potentials were needed to reproduce the observed lowest single-particle energy in the $^{208}_{\Lambda}$Pb hypernucleus, as well as the energy difference between the Λ and Σ hyperons obtained in the G-matrix calculation in nuclear matter [38], in addition to the effective Lagrangian density, Eq. (3). But these repulsive "Pauli" (vector) potentials will be included in the explicit density-dependent parametrizations, while the one-gluon exchange interaction in medium, that yields agreement with "no experimental observation of the Σ hypernuclei," will not be included, where the interaction was introduced in the latest version of the QMC model [39]. Thus, in order to agree with this fact, we will include a phenomenological repulsive vector potential for the Σ, in such a way that it yields the Σ total potential of $\sim + 30$ MeV at ρ_0; the corresponding parametrizations for the vector potential will also be given.

The coupling constants of the hyperon appearing in Eq. (3) are $g_\omega^Y = (n_q/3)g_\omega$ and $g_\rho^Y \equiv g_\rho = g_\rho^q$, with n_q being the number of valence light quarks in the hyperon Y ($n_q = 3$ for N), where g_ω and g_ρ, which appear in Eq. (2), are the ω–N and ρ–N coupling constants, respectively. I_3^Y and Q_Y are the third component of the hyperon isospin operator and the electric charge in units of the positron charge, e, respectively. The couplings between the meson fields and quarks, as already mentioned, reflect the fact that the magnitude of the light quark condensates is expected to reduce faster than those of the strange and heavier quarks as baryon (nuclear) density increases.

The σ-field-dependent σ–N [σ–Y] coupling strength for the nucleon N [hyperon Y], $g_\sigma^N(\sigma)$ [$g_\sigma^Y(\sigma)$], implicit in Eq. (2) [Eq. (3)], is defined by

$$m_{N,Y}^*(\sigma) \equiv m_{N,Y} - g_\sigma^{N,Y}(\sigma)\sigma(\vec{r}) \qquad (Y = \Lambda, \Sigma, \Xi, \Delta, \Sigma^*, \Xi^*, \Lambda_c, \Sigma_c, \Xi_c, \Lambda_b, \Sigma_b, \Xi_b), \quad (4)$$

where m_N [m_Y] is the free nucleon [hyperon] mass. Note that the dependence of the coupling strengths on the scalar field σ must be calculated self-consistently within the quark model [22,33,38,40,41,49] (the MIT bag model in the present case). This characterizes the QMC model differently from quantum hadrodynamics (QHD) [134,135], as well as from other naive symmetry-based approaches. Namely, although in such approaches $g_\sigma^Y(\sigma)/g_\sigma^N(\sigma)$ may be 2/3 or 1/3 depending on the number of light quarks n_q in the hyperon Y in free space (means $\sigma = 0$), this may not be true any more in a nuclear medium. (Even in free space this is not true, since the bag radii of the nucleon and hyperon are not exactly the same [38,136].)

For later convenience, we define $C_{N,Y}(\sigma) \equiv S_{N,Y}(\sigma)/S_{N,Y}(\sigma = 0)$ and $S_{N,Y}(\sigma)$ in connection with $m_{N,Y}^*$ [21], denoting the light quarks by $q(\equiv u, d)$, as

$$\frac{dm_{N,Y}^*(\sigma)}{d\sigma} = -n_q g_\sigma^q \int_{bag} d^3y\, \overline{\psi}_q(\vec{y})\psi_q(\vec{y})$$

$$\equiv -n_q g_\sigma^q S_{N,Y}(\sigma) = -\left[n_q g_\sigma^q S_{N,Y}(\sigma = 0)\right]\left(\frac{S_{N,Y}(\sigma)}{\left[n_q g_\sigma^q S_{N,Y}(\sigma = 0)\right]}\right)$$

$$\equiv -\left[n_q g_\sigma^q S_{N,Y}(\sigma = 0)\right] C_{N,Y}(\sigma) = -\frac{d}{d\sigma}\left[g_\sigma^{N,Y}(\sigma)\sigma\right], \quad (5)$$

where g_σ^q is the (light quark)–σ coupling constant, and ψ_q is the light quark ground state wave function in N or Y immersed in a nuclear medium, where the in-medium masses $m_{N,Y}^*$ are associated with the *quark scalar charge*. The σ–N and σ–Y coupling constants in free space (i.e. $\sigma = 0$) are defined by

$$g_\sigma^{N,Y} \equiv g_\sigma^{N,Y}(\sigma = 0) \equiv n_q g_\sigma^q S_{N,Y}(\sigma = 0). \quad (6)$$

Note that the values of $S_N(\sigma)$ and $S_Y(\sigma)$ in Eq. (5) are different, since the light quark ground state wave functions in N and Y are different in free space and in medium. Since the light quarks in any hadrons are expected to feel the same scalar and vector potentials as those in the nucleon, one can systematically study the hadron properties in medium using the same (light quark)–meson coupling constants, which are constrained by the nuclear matter saturation properties. This is one of the big advantages of the QMC model.

Next, we consider the rest frame of symmetric nuclear matter, a spin and isospin saturated, infinitely large system with only the strong interaction. In this case, the self-consistent effect from the embedded one-hyperon to the (nuclear matter + one hyperon) system can be neglected, although for a hypernucleus, the effect is self-consistently included together with the influence of the Pauli potentials and channel couplings as a $1/A$ effect, with A being the total baryon number of the hypernucleus (see Refs. [21,22,38,64] for details). Thus, the quark–meson coupling constants that are determined by the saturation properties of symmetric nuclear matter (without a hyperon), as well as the total energy per nucleon, will not be affected in the (nuclear matter + one hyperon) system.

The Dirac equations for the quarks and antiquarks in nuclear matter, in a bag of a hadron h ($q = u$ or d, and $Q \equiv s, c$ or b, hereafter), are given, for $x = (t, \vec{x})$ and $|\vec{x}| \le$ bag radius [44,47–50], by

$$\left[i\gamma \cdot \partial_x - (m_q - V_\sigma^q) \mp \gamma^0 \left(V_\omega^q + \frac{1}{2} V_\rho^q \right) \right] \begin{pmatrix} \psi_u(x) \\ \psi_{\bar{u}}(x) \end{pmatrix} = 0, \tag{7}$$

$$\left[i\gamma \cdot \partial_x - (m_q - V_\sigma^q) \mp \gamma^0 \left(V_\omega^q - \frac{1}{2} V_\rho^q \right) \right] \begin{pmatrix} \psi_d(x) \\ \psi_{\bar{d}}(x) \end{pmatrix} = 0, \tag{8}$$

$$\left[i\gamma \cdot \partial_x - m_Q \right] \psi_Q(x) = 0, \qquad \left[i\gamma \cdot \partial_x - m_Q \right] \psi_{\overline{Q}}(x) = 0, \tag{9}$$

where the mean field potentials are defined by $V_\sigma^q \equiv g_\sigma^q \sigma$, $V_\omega^q \equiv g_\omega^q \omega$, and $V_\rho^q \equiv g_\rho^q b$, with g_σ^q, g_ω^q, and g_ρ^q being the corresponding quark–meson coupling constants. We assume SU(2) symmetry, $m_{u,\bar{u}} = m_{d,\bar{d}} \equiv m_{q,\bar{q}}$. The Lorentz-scalar "effective quark masses" are defined by $m_{u,\bar{u}}^* = m_{d,\bar{d}}^* = m_{q,\bar{q}}^* \equiv m_{q,\bar{q}} - V_\sigma^q$, and thus m_q^* is dominated by $-V_\sigma^q$ as baryon density increases, and can be negative. Note that $m_Q = m_Q^*$, since the σ field does not couple to the heavier quarks $Q = s$, c, b. Furthermore, since the ρ-meson mean field becomes zero, $V_\rho^q = 0$, in Eqs. (7) and (8) in symmetric nuclear matter in the Hartree approximation, we will ignore it.

The same mean fields σ and ω for the quarks in Eqs. (7) and (8), satisfy self-consistently the following equations at the nucleon level, with $m_N^*(\sigma)$ to be calculated by Eq. (13):

$$\omega = \frac{g_\omega}{m_\omega^2} \rho_B \equiv \frac{g_\omega}{m_\omega^2} \frac{4}{(2\pi)^3} \int d^3k \, \theta(k_F - |\vec{k}|), \tag{10}$$

$$\sigma = \frac{g_\sigma^N}{m_\sigma^2} C_N(\sigma) \rho_s \equiv \frac{g_\sigma^N}{m_\sigma^2} C_N(\sigma) \frac{4}{(2\pi)^3} \int d^3k \, \theta(k_F - |\vec{k}|) \frac{m_N^*(\sigma)}{\sqrt{m_N^{*2}(\sigma) + \vec{k}^2}}, \tag{11}$$

where k_F is the nucleon Fermi momentum.

Because of the underlying quark structure of the nucleon used to calculate $m_N^*(\sigma)$ in the nuclear medium, $C_N(\sigma)$ decreases as σ increases, whereas in the usual point-like nucleon $C_N(\sigma) = 1$. It is this variation of $C_N(\sigma)$ (or equivalently the σ-dependence of the coupling as $g_\sigma^N(\sigma(\rho_B))$) that yields a novel saturation mechanism for nuclear matter—σ-dependence originates from the quark structure of the nucleon. The important dynamics, which originates from the quark structure of the nucleon, is included in $C_N(\sigma)$. This $C_N(\sigma)$ also yields three-body or density-dependent effective forces at the nucleon level [66,137]. As a consequence, the QMC model gives a nuclear incompressibility of $K \simeq 280$ MeV with the free space inputs $m_q = 5$ MeV and nucleon bag radius 0.8 fm [64]. This value is in contrast to a naive version of QHD [134,135] that results in much larger value, $K \simeq 500$ MeV, where the empirically extracted value falls in the range $K = 200$–300 MeV. (See Ref. [138] for details.)

Once the self-consistency equation for the σ field in Eq. (11) is solved, one can calculate the total energy per nucleon:

$$E^{\text{tot}}/A = \frac{4}{(2\pi)^3 \rho_B} \int d^3k \, \theta(k_F - |\vec{k}|) \sqrt{m_N^{*2}(\sigma) + \vec{k}^2} + \frac{m_\sigma^2 \sigma^2}{2\rho_B} + \frac{g_\omega^2 \rho_B}{2m_\omega^2}. \tag{12}$$

The parameters appearing in the Lagrangian density of Eqs. (1)–(3), and also above, are $m_\omega = 783$ MeV, $m_\rho = 770$ MeV, $m_\sigma = 550$ MeV, and $e^2/4\pi = 1/137.036$ [33,34]. The coupling constants, $g_\sigma^N \equiv g_\sigma$, $g_\omega^N \equiv g_\omega$, and $g_\rho^N \equiv g_\rho$ at the nucleon level, are determined by the fit to the binding energy of 15.7 MeV at the saturation density $\rho_0 = 0.15$ fm^{-3} ($k_F^0 = 1.305$ fm^{-1}) for symmetric nuclear matter, as well as g_ρ to the symmetry energy of 35 MeV. The corresponding quark–meson coupling constants determined, and the current quark mass values (inputs), respectively denoted by "Set I" and "Set II," are listed in Tables 1 and 2, where in Set I the current quark mass values of the strange (m_s) and bottom (m_b) quarks are different from those

Table 1. (Set I) Current quark mass values (inputs), quark–meson coupling constants, and the bag constant B_p [21], obtained with the following inputs: free nucleon bag radius $R_N = 0.8$ fm, empirical values $E^{tot}/A - m_N = -15.7$ MeV ($m_N = 939$ MeV) at the saturation density $\rho_0 = 0.15$ fm^{-3}, and a symmetry energy of 35 MeV.

$m_{u,d}$	5 MeV	g_σ^q	5.69
m_s	250 MeV	g_ω^q	2.72
m_c	1270 MeV	g_ρ^q	9.33
m_b	4200 MeV	$B_p^{1/4}$	170 MeV

Table 2. (Set II) As Table 1, but the current quark mass values for the strange (m_s) and bottom (m_b) quarks are from Ref. [139].

$m_{u,d}$	5 MeV	g_σ^q	5.69
m_s	93 MeV	g_ω^q	2.72
m_c	1270 MeV	g_ρ^q	9.33
m_b	4180 MeV	$B_p^{1/4}$	170 MeV

in Ref. [139]. Although the (current) quark mass values in effective models do not have direct connections with those in QCD, we use the latest values quoted in Ref. [139] for Set II, where one may see a model parameter dependence in the Set I and Set II results. Note that the current quark mass values, except for the u and d quarks, do not influence the nuclear matter saturation properties, thus the relevant quark–meson coupling constants, g_σ^q, g_ω^q, and g_ρ^q, are the same in Tables 1 and 2. In the past, including Ref. [21], use of the strange quark current mass value of $m_s = 250$ MeV was motivated by the success in reproducing the light hadron masses in the MIT bag model with $m_s = 279$ MeV [151]. In the present study we also use different values for the strange and bottom quark current masses, respectively $m_s = 93$ MeV and $m_b = 4180$ MeV (Set II) given in Ref. [139].

The corresponding coupling constant values at the nucleon level are $g_\sigma^2/4\pi = (g_\sigma^N)^2/4\pi = 5.39$ (see Eq. (6) with $S_N(0) = 0.4827$, where Ref. [21] mistakenly gave the value for finite nuclei), $g_\omega^2/4\pi = (g_\omega^N)^2/4\pi = (3g_\omega^q)^2/4\pi = 5.30$, and $g_\rho^2/4\pi = (g_\rho^N)^2/4\pi = (g_\rho^q)^2/4\pi = 6.93$.

The mass of a hadron h in symmetric nuclear matter, m_h^* (free mass is m_h), is calculated, together with the mass stability condition with respect to the in-medium bag radius at a given density:

$$m_h^* = \sum_{j=q,\bar{q},Q,\bar{Q}} \frac{n_j \Omega_j^* - z_h}{R_h^*} + \frac{4}{3}\pi R_h^{*3} B_p, \qquad \frac{dm_h^*}{dR_h^*} = 0, \qquad (13)$$

where $\Omega_q^* = \Omega_{\bar{q}}^* = [(x_q^*)^2 + (R_h^* m_q^*)^2]^{1/2}$ ($q = u, d$), with $m_q^* = m_q - g_\sigma^q \sigma = m_q - V_\sigma^q$, $\Omega_Q^* = \Omega_{\bar{Q}}^* = [(x_Q^*)^2 + (R_h^* m_Q)^2]^{1/2}$ ($Q = s, c, b$), and $x_{q,Q}^*$ are the lowest-mode bag eigenfrequencies. B_p is the bag constant (assumed to be independent of density), $n_{q,Q}[n_{\bar{q},\bar{Q}}]$ are the lowest-mode valence quark [antiquark] numbers of each quark flavor $q = (u, d)$, $Q = (s, c, b)$ in the hadron h, while z_h parametrizes the sum of the center-of-mass and gluon fluctuation effects, which is assumed to be independent of density [33]. The bag constant $B_p = (170 \text{ MeV})^4$ is determined by the free nucleon mass $m_N = 939$ MeV, free nucleon bag radius $R_N = 0.8$ fm, and $m_q = 5$ MeV, which are considered to be the standard input values in the QMC model [64]. Recall that the quark–meson coupling constants, g_σ^q, g_ω^q, and g_ρ^q, have already been determined by the nuclear

matter saturation properties; we can use the same coupling constants, which are empirically constrained, for the light quarks in any hadrons.

The calculated effective baryon and meson scalar potentials $[m_B^* - m_B]$ and $[m_M^* - m_M]$ are shown in Figs. 1 and 2 respectively, simply denoted by $[m^* - m]$, for both Set I (left panel) and Set II (right panel). One can notice that the "light quark number counting rule," namely that the Lorentz-scalar potential is proportional to the number of light quarks in the hadron, is realized well for both the baryon and meson cases. (The η and η' meson cases will be discussed later.)

The ground state wave function of the quark q or Q in the hadron h immersed in the nuclear medium satisfies the boundary condition at the bag surface,

$$j_0(x_{q,Q}^*) = \beta_{q,Q}^{h*} j_1(x_{q,Q}^*), \tag{14}$$

where $j_{0,1}$ are the spherical Bessel functions, and

$$\beta_q^{h*} = \sqrt{\frac{\Omega_q^* - m_q^* R_h^*}{\Omega_q^* + m_q^* R_h^*}}, \qquad \beta_Q^{h*} = \sqrt{\frac{\Omega_Q^* - m_Q R_h^*}{\Omega_Q^* + m_Q R_h^*}}. \tag{15}$$

The ground state quark wave functions $\psi_{q,Q}^{B*}(\vec{r})$ in a baryon B in symmetric nuclear matter are given by replacing $h \to B$ in the above,

$$\psi_{q,Q}^{B*}(\vec{r}) = N_{q,Q}^{B*} \begin{pmatrix} j_0\left(x_{q,Q}^* r/R_B^*\right) \\ i\,\beta_{q,Q}^{B*}\,\vec{\sigma}\cdot\hat{r}\,j_1\left(x_{q,Q}^* r/R_B^*\right) \end{pmatrix} \frac{\chi_s}{\sqrt{4\pi}}, \tag{16}$$

with

$$\left(N_{q,Q}^{B*}\right)^{-2} = 2\left(R_B^*\right)^3 j_0^2\left(x_{q,Q}^*\right)\left[\Omega_{q,Q}^*\left(\Omega_{q,Q}^* - 1\right) + m_{q,Q}^* R_B^*/2\right]/x_{q,Q}^{*2}, \tag{17}$$

where $r = |\vec{r}|$, $\hat{r} = \vec{r}/r$, $m_Q^* = m_Q$ as already mentioned, and χ_s is the Pauli spinor.

2.2 *Density-dependent parametrizations*

In connection with the Lorentz-scalar potentials $[m_B^* - m_B] = -g_\sigma^{B=N,Y}(\sigma)\sigma$ shown in Fig. 1 (or equivalently the effective baryon masses m_B^*), it has been found that the function $C_B(\sigma)(B = N, \Lambda, \Sigma, \Xi, \Delta, \Sigma^*, \Xi^*, \Lambda_c, \Sigma_c, \Xi_c, \Lambda_b, \Sigma_b, \Xi_b)$ appearing in the last line in Eq. (5) can be parametrized as a linear form in the σ field, $g_\sigma^N \sigma = g_\sigma^N(\sigma = 0)\sigma$, as shown in Fig. 3, for practical purposes [33,34,38],

$$C_B(\sigma) = 1 - a_B \times \left(g_\sigma^N \sigma\right), \qquad (B = N, \Lambda, \Sigma, \Xi, \Delta, \Sigma^*, \Xi^*, \Lambda_c, \Sigma_c, \Xi_c, \Lambda_b, \Sigma_b, \Xi_b), \tag{18}$$

where we compare with the σ-dependent coupling case, $g_\sigma^N(\sigma)\sigma$, and without the dependent case, $g_\sigma^N \sigma = g_\sigma^N(\sigma = 0)\sigma$, in the left panel of Fig. 3.

The values obtained for a_B are listed in Tables 3 and 4 for Sets I and II respectively. Note that for the antibaryon $\overline{B}$, $a_{\overline{B}} = a_B$, and also $m_{\overline{B}}^* = m_B^*$ with $n_q \to n_{\overline{q}}$ below. This parametrization works very well up to about three times the normal nuclear matter density, $3\rho_0$. Then, the effective mass of baryon B in nuclear matter, where $m_B^* - m_B$ are shown in Fig. 1, is approximated well by the following (the accuracy will be discussed in the last part of this subsection):

$$m_B^* \simeq m_B - \frac{n_q}{3} g_\sigma^N \left[1 - \frac{a_B}{2}\left(g_\sigma^N \sigma\right)\right]\sigma = m_B - \frac{n_q}{3}\left[\left(g_\sigma^N \sigma\right) - \frac{a_B}{2}\left(g_\sigma^N \sigma\right)^2\right] \tag{19}$$

$$(B = N, \Lambda, \Sigma, \Xi, \Delta, \Sigma^*, \Xi^*, \Lambda_c, \Sigma_c, \Xi_c, \Lambda_b, \Sigma_b, \Xi_b),$$

with n_q being the valence light quark number in the baryon B, where $g_\sigma^N \sigma = g_\sigma^N(\sigma = 0)\sigma$ (in MeV) can be fitted (parametrized) well as a function of x for $0 \le x = \rho_B/\rho_0 \le 3.0$
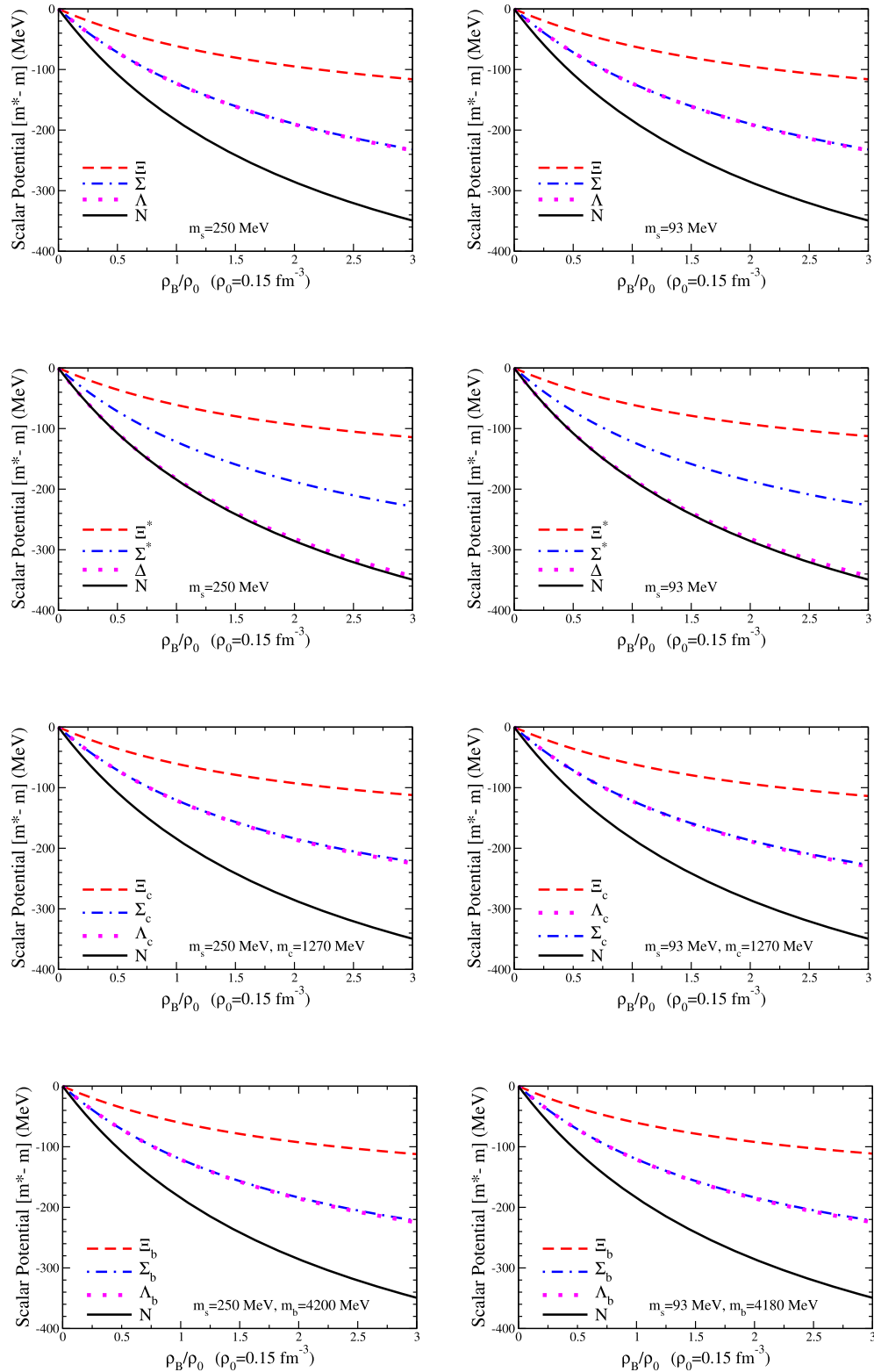
Fig. 1. Density dependence of the baryon scalar potentials, $[m^* - m]$, for the octet, decuplet, low-lying charm, and low-lying bottom baryons, for Set I (left panel) and Set II (right panel).
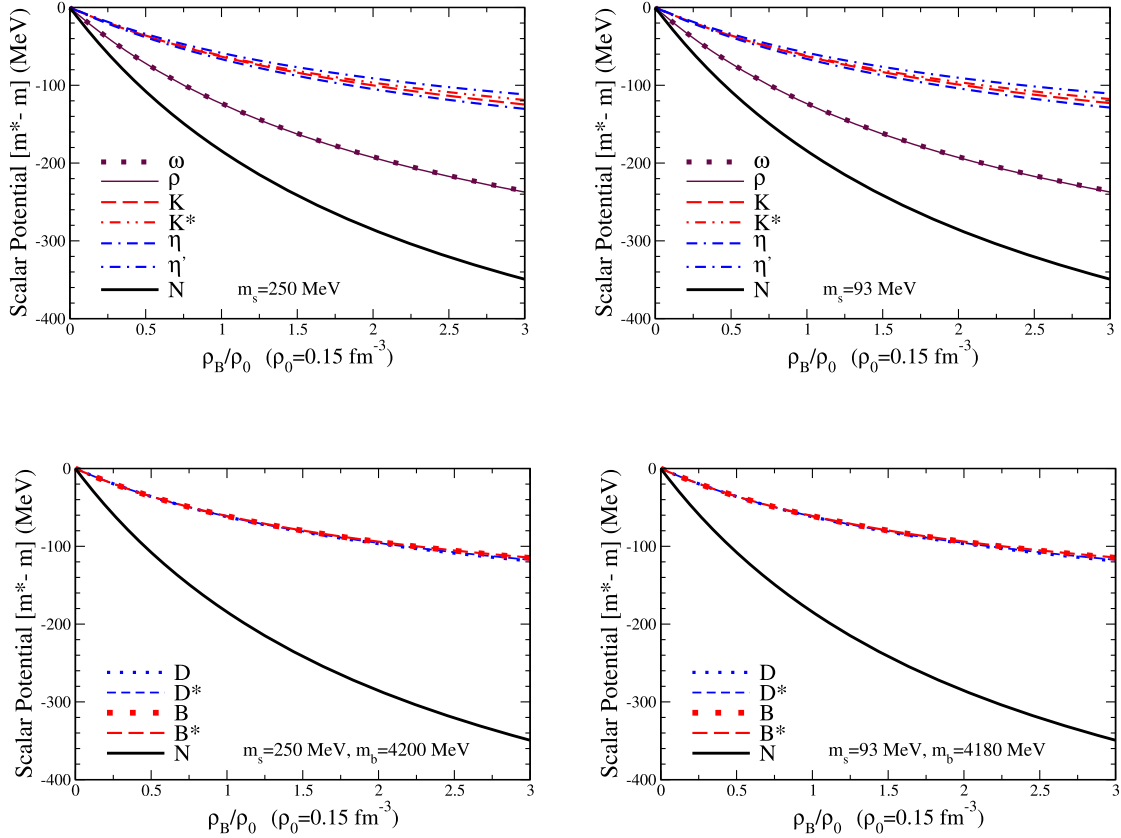
Fig. 2. Density dependence of the meson scalar potentials, $[m^* - m]$, for the light and strange mesons (upper panel) and the charm and bottom mesons (lower panel), for Set I (left panel) and Set II (right panel). Note that for the η and η' mesons the pseudoscalar octet(8)–singlet(1) mixing angle of $\theta_P = -11.3°$ from the linear mass formula [139] is used. This makes the effective mass of η (η') lighter (heavier) than that of η_8 (η_1), where the possible density dependence of the mixing angle for θ_P is ignored.

Fig. 3. Density dependence of $-g_\sigma^N(\sigma)\sigma$ and $-g_\sigma^N(\sigma = 0)\sigma = -g_\sigma^N\sigma$ (left panel) and the fit result for $g_\sigma^N(\sigma = 0)\sigma = g_\sigma^N\sigma$ (right panel).

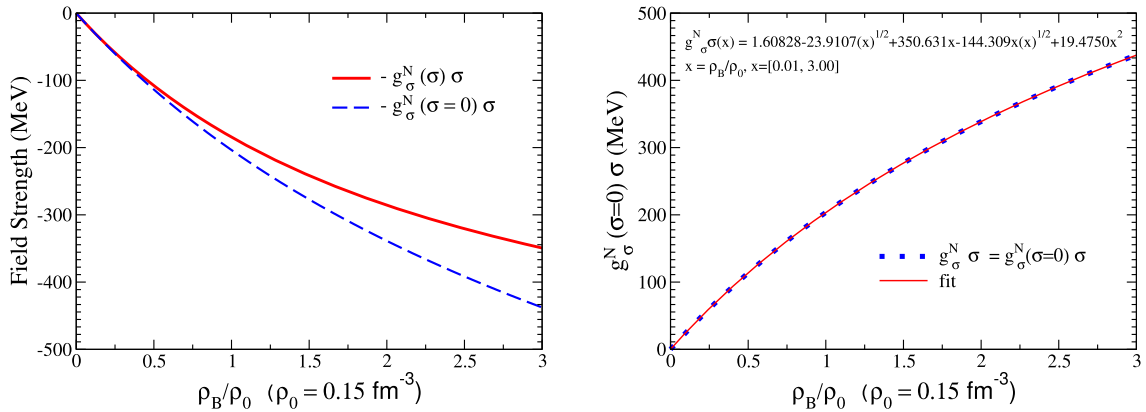**Table 3.** (Set I) Effective mass slope parameter a_B [Eq. (19)] and the vector potential parameter b_B [Eq. (23)] for $B = N, \Lambda, \Sigma, \Xi, \Delta, \Sigma^*, \Xi^*, \Lambda_c, \Sigma_c, \Xi_c, \Lambda_b, \Sigma_b, \Xi_b$, and the effective mass slope parameter a_M [Eq. (25)] for $M = \omega, \rho, K, K^*, \eta, \eta', D, D^*, B, B^*$. Note that the tiny differences in the values of a_B from those in Refs. [64,65] are due to the differences in the number of data points for calculating a_B, but such differences give negligible effects. Concerning the Σ vector potential, the alternative parametrization $\tilde{b}_\Sigma$ yields a total potential of $[m_\Sigma^* - m_\Sigma] + V_v^\Sigma \simeq +30\,\mathrm{MeV}$ at ρ_0.

a_B	$\times 10^{-4}\,\mathrm{MeV}^{-1}$	a_B	$\times 10^{-4}\,\mathrm{MeV}^{-1}$	a_B	$\times 10^{-4}\,\mathrm{MeV}^{-1}$	a_B	$\times 10^{-4}\,\mathrm{MeV}^{-1}$
a_N	9.15	a_Δ	10.08	–	–	–	–
a_Λ	9.35	–	–	a_{Λ_c}	9.90	a_{Λ_b}	10.78
a_Σ	9.59	a_{Σ^*}	10.15	a_{Σ_c}	10.34	a_{Σ_b}	11.22
a_Ξ	9.52	a_{Ξ^*}	10.15	a_{Ξ_c}	9.99	a_{Ξ_b}	10.83
b_B	MeV	b_B	MeV	b_B	MeV	b_B	MeV
b_N	125.30	b_Δ	125.30	–	–	–	–
b_Λ	92.57	–	–	b_{Λ_c}	83.54	b_{Λ_b}	83.54
b_Σ	100.12	b_{Σ^*}	83.54	b_{Σ_c}	83.54	b_{Σ_b}	83.54
$\tilde{b}_\Sigma$	152.42						
b_Ξ	46.29	b_{Ξ^*}	41.77	b_{Ξ_c}	41.77	b_{Ξ_b}	41.77
a_M	$\times 10^{-4}\,\mathrm{MeV}^{-1}$	a_M	$\times 10^{-4}\,\mathrm{MeV}^{-1}$	a_M	$\times 10^{-4}\,\mathrm{MeV}^{-1}$	a_M	$\times 10^{-4}\,\mathrm{MeV}^{-1}$
a_ω	8.73	a_K	6.66	a_D	8.61	a_B	9.92
a_ρ	8.70	a_{K^*}	8.60	a_{D^*}	9.09	a_{B^*}	10.04
–	–	$a_\eta(n_q^\eta \to 1)$	7.03	–	–	–	–
–	–	$a_{\eta'}(n_q^{\eta'} \to 1)$	8.81	–	–	–	–

Table 4. (Set II) As Table 3, but for the parameters in Set II.

a_B	$\times 10^{-4}\,\mathrm{MeV}^{-1}$	a_B	$\times 10^{-4}\,\mathrm{MeV}^{-1}$	a_B	$\times 10^{-4}\,\mathrm{MeV}^{-1}$	a_B	$\times 10^{-4}\,\mathrm{MeV}^{-1}$
a_N	9.15	a_Δ	10.08	–	–	–	–
a_Λ	9.68	–	–	a_{Λ_c}	9.90	a_{Λ_b}	10.82
a_Σ	9.91	a_{Σ^*}	10.44	a_{Σ_c}	10.34	a_{Σ_b}	11.27
a_Ξ	10.15	a_{Ξ^*}	10.71	a_{Ξ_c}	10.28	a_{Ξ_b}	11.13
b_B	MeV	b_B	MeV	b_B	MeV	b_B	MeV
b_N	125.30	b_Δ	125.30	–	–	–	–
b_Λ	92.57	–	–	b_{Λ_c}	83.54	b_{Λ_b}	83.54
b_Σ	100.12	b_{Σ^*}	83.54	b_{Σ_c}	83.54	b_{Σ_b}	83.54
$\tilde{b}_\Sigma$	152.00						
b_Ξ	46.29	b_{Ξ^*}	41.77	b_{Ξ_c}	41.77	b_{Ξ_b}	41.77
a_M	$\times 10^{-4}\,\mathrm{MeV}^{-1}$	a_M	$\times 10^{-4}\,\mathrm{MeV}^{-1}$	a_M	$\times 10^{-4}\,\mathrm{MeV}^{-1}$	a_M	$\times 10^{-4}\,\mathrm{MeV}^{-1}$
a_ω	8.73	a_K	7.24	a_D	8.61	a_B	9.97
a_ρ	8.70	a_{K^*}	8.99	a_{D^*}	9.09	a_{B^*}	10.10
–	–	$a_\eta(n_q^\eta \to 1)$	7.54	–	–	–	–
–	–	$a_{\eta'}(n_q^{\eta'} \to 1)$	9.20	–	–	–	–

$(\rho_0 = 0.15\,\mathrm{fm}^{-3})$ as

$$(g_\sigma^N \sigma)(x) = \begin{cases} 1.60828 - 23.9107\sqrt{x} + 350.631x \\ \qquad - 144.309x\sqrt{x} + 19.4750x^2 \quad (x > 0), \\ 0 \qquad\qquad\qquad\qquad\qquad\qquad (x = 0), \end{cases} \tag{20}$$

with χ^2/d.o.f. $= 0.06653/301$, where $0.01 \leq x$ in practice, and the fitted result is shown in the right panel of Fig. 3. Then, using Eq. (19) and the a_B values given in Tables 3 and 4, one can obtain the corresponding effective mass values m_B^* for a given baryon density ρ_B (fm^{-3}); in particular, that for N, m_N^* with $a_N = 9.15 \times 10^{-4}\,\mathrm{MeV}^{-1}$ and $n_q = 3$ may be useful.

Furthermore, the Lorentz-vector-isoscalar ω mean field potential V_ω^B $[V_v^h]$ (in MeV) for a baryon B [hadron h], and the ω potential for the light quarks ($q = u, d$) V_ω^q (MeV) can also be parametrized using $x = \rho_B/\rho_0$ ($\rho_0 = 0.15\,\mathrm{fm}^{-3}$) as

$$V_\omega^B(x) = b_B x, \tag{21}$$

$$V_\omega^q(x) = 41.77x, \tag{22}$$

$$V_v^h(x) = V_\omega^h = (n_q - n_{\bar{q}})V_\omega^q = (n_q - n_{\bar{q}}) \times 41.77x \quad \text{(except for the baryon octet)}, \tag{23}$$

where the values of b_B are the same for both Sets I and II, and are given in Tables 3 and 4, respectively. Note that for Λ, Σ, and Ξ hyperons, phenomenologically introduced quark-based "Pauli potentials" [38] are included in b_B, assuming the same for both Sets I and II. As for the Σ total potential in a nonrelativistic sense to apply for the upper component of the Dirac spinor, $[m_\Sigma^* - m_\Sigma] + V_v^\Sigma$ at ρ_0, the above parametrizations give an attractive potential of $\sim\!-22\,\mathrm{MeV}$ for both Sets I and II. If we want to agree with the "no experimental observation of the Σ hypernuclei," we need to introduce the alternative, phenomenological parametrizations to yield, e.g., $[m_\Sigma^* - m_\Sigma] + V_v^\Sigma \simeq +30\,\mathrm{MeV}$ at ρ_0, and we give the results in Tables 3 and 4 for this case denoted by $\tilde{b}_\Sigma$.

For completeness, we also give the Lorentz-vector-isovector mean field potential (in MeV) as a function of $y \equiv \rho_3/\rho_0 = (\rho_p - \rho_n)/\rho_0$ with the isospin-third component of the hadron h, I_3^h,

$$I_3^h V_\rho^h(y) = I_3^h \times 84.61y, \tag{24}$$

where the expression given in Ref. [64] wrongly contained a factor of 1/2.

Similarly, by defining $n_q^M \equiv (n_q + n_{\bar{q}})$, and using $a_M = a_{\overline{M}}$, the effective masses of the low-lying mesons m_M^* ($M = \omega, \rho, K, K^*, \eta, \eta', D, D^*, B, B^*$) are given below, except for the pion, which is the (nearly) Goldstone boson and difficult to describe consistently in naive independent/additive quark models (the pion mass is not expected to be modified up to about normal nuclear matter density [140–142]):

$$m_M^* \simeq m_M - \frac{n_q^M}{3}g_\sigma^N\left[1 - \frac{a_M}{2}(g_\sigma^N\sigma)\right]\sigma = m_M - \frac{n_q^M}{3}\left[(g_\sigma^N\sigma) - \frac{a_M}{2}(g_\sigma^N\sigma)^2\right]$$

$$(M = \omega, \rho, K, K^*, \eta, \eta', D, D^*, B, B^*, \text{ with } n_q^M \to 1 \text{ for } \eta \text{ and } \eta'). \tag{25}$$

In the above, $n_q^M = n_q^{\eta,\eta'} \to 1$ for the η and η' mesons may be verified from Fig. 2, where the pseudoscalar octet(8)–singlet(1) mixing angle of $\theta_P = -11.3°$ from the linear mass formula [139] is used. This makes the effective mass of η (η') lighter (heavier) than that of η_8 (η_1), neglecting the possible density dependence of the mixing angle θ_P, as also shown explicitly in Refs. [45,46,64] by the effective mass ratios. $n_q^{\eta,\eta'} \to 1$ for η and η' reflects the fact that the numerator of the total energy for the η and η' in Eq. (13) becomes nearly the sum, $\sim(\Omega_q^* + \Omega_s^*)$, when the flavor octet and singlet wave functions are used with the mixing effect of $\theta_P = -11.3°$, which is different from the ϕ–ω ideal-mixing case. Note that the ω and ρ mesons appearing above are the those of the SU(6) quark model, and should not be confused with the ω and ρ (mean) fields in the QMC model. The obtained slope parameters a_M are listed in Tables 3 and 4 for Sets I

and II respectively. Note that the ω mean field potential for the kaon (K) in the QMC model must be modified as

$$V_\omega^K(x) \simeq 1.96 \times 41.77x \tag{26}$$

to reproduce the empirically extracted repulsive K^+ total potential [44] for both Sets I and II. This gives the total K^+ potential of $\sim + 19$ MeV at ρ_0 for both sets.

We comment briefly on the accuracy of the parametrizations given above. Since the vector potentials are proportional to the baryon density ρ_B or $\rho_3 = \rho_p - \rho_n$, the parametrizations are simple and should be good. For the effective masses of the baryons and mesons, the quality of the parametrizations with a_B, a_M, and $(g_\sigma^N \sigma)(x)$ of Eq. (20) are all well within 1.0% deviations from the calculated results for $0.01 \leq \rho_B/\rho_0 \leq 3.0$, except that m_η^* has a maximum of 1.7% deviation ($\simeq 7$ MeV) from the original result. Thus, for practical purposes, one can comfortably use the given parametrizations for the effective masses (Lorentz-scalar-isoscalar potentials) of the baryons and mesons for a given baryon density for $0.01 \leq \rho_B/\rho_0 \leq 3.0$, as well as for the Lorentz-vector-isoscalar and Lorentz-vector-isovector mean field potentials. Recall that the η and $\eta^{'}$ cases are subject to the mixing of the octet and the singlet states, and also $n_q \to 1$ is applied for them. However, the observed maximum deviation of 1.7% from their parametrizations are surprisingly good.

3. Baryon magnetic moments in symmetric nuclear matter

In Ref. [21] we obtained the MIT bag model wave functions in symmetric nuclear matter for the octet, low-lying charm, and low-lying bottom baryons with nonzero light quarks with the Set I current quark mass values (Table 1). In this study we extend further to include the decuplet baryons for Set I as well as for Set II, and calculate the wave functions of the octet, decuplet, low-lying charm, and low-lying bottom baryons with nonzero light quarks also for Set II (Table 2). Below, we calculate the magnetic moments of these baryons and some transition magnetic moments in symmetric nuclear matter using the MIT bag (QMC model) wave functions in Set I (Table 1) and Set II (Table 2).

First, we discuss the magnetic moment of an octet baryon B, μ_B, in free space (vacuum). For the octet baryons $B(q_1, q_2, q_3)$, specifying by this the quark order, the familiar SU(6) flavor–spin wave functions are constructed based on the isospin, spin, and Pauli principle, and are consistent with the "1–2 quark order" for the quarks q_1 and q_2, namely, the first two quarks q_1 and q_2 are the closest in mass [106]. Good examples may be the wave functions of the Λ and Σ^0 baryons. The first two quarks $(q_1, q_2) = (u, d)$ are antisymmetric in the Λ but symmetric in the Σ^0. Similar arguments may not necessarily be applicable for the baryons with c and/or b quarks with nonzero light quarks, in particular for the baryons such as $B(q_1, q_2, q_3)(q_1 = q, q_2 = Q \neq q_3 = Q^{'})$, since isospin symmetry and the Pauli principle cannot help. As discussed in Ref. [106], different assignments for the quarks q_1, q_2, and q_3 in $B(q_1, q_2, q_3)(q_{1, 2, 3} = q, Q)$ are possible in some cases without violating the Pauli principle, and the different assignments give different results for the calculated magnetic moments. This applies to the $\Xi_{c, b}$ baryons in the present study. Although the first two quark pairs (u, s) or (d, s) are antisymmetric in the low-lying $\Xi_{c,b}$ baryons [132], these cases agree with the assumption of the "1–2 quark order" for these heavy baryons—as a natural assumption, the same as that for the octet baryons. Despite some discussions in Ref. [106] of the quark order, we take the quarks q_1 and q_2 as the closest in mass in the wave functions. In these cases, the $\Xi_{c,b}$ wave functions have a similar structure

to those of the $\Lambda_{c,b}$ baryons. Note that the "1–2 quark order" is supported in Ref. [106] as the best quark ordering for flavor-degenerate baryons for the masses.

The magnetic moment μ_B of the baryon $B(q_1, q_2, q_3)$ in an impulse approximation (independent quark picture) is expressed in terms of the jth quark magnetic moments $\mu_j(j = 1, 2, 3)$:

$$\mu_B = \frac{1}{3}(2\mu_1 + 2\mu_2 - \mu_3) \qquad (B \neq \Lambda, \Lambda_{c,b} \neq \text{decuplet}), \tag{27}$$

$$\mu_B = \mu_3 \qquad (B = \Lambda, \Lambda_{c,b}, \Xi_{c,b}), \tag{28}$$

$$\mu_B = \mu_1 + \mu_2 + \mu_3 \qquad (B = \text{decuplet}), \tag{29}$$

where we ignore any possible opposite parity state mixing, isospin mixing, and flavor mixing. Note that in Eq. (28) the quark order q_1 and q_2 is implied in such a way that they are coupled to an isospin-0 and spin-0 pair, and the notation $B(q_1, q_2, q_3)$ indicates this (in Tables 5 and 6). We give explicit expressions for the baryon magnetic moments and the transition magnetic moments in the second columns of Tables 5 and 6 for Sets I and II respectively.

Next, as an example, we discuss the magnetic moment of a light quark q in a baryon B in the MIT bag model. For a heavy quark Q in B, one may replace $q \to Q$ with the corresponding quantities. The free space magnetic moment of the light quark μ_q with charge e_q in the baryon B is given by

$$\mu_q \equiv e_q \eta_q \equiv e_q \left[(N_q^B)^2 \int_0^{R_B} dr\, r^2\, \frac{2r}{3}\, j_0(x_q r/R_B)\, \beta_q^B\, j_1(x_q r/R_B) \right], \tag{30}$$

where R_B is the bag radius of the baryon B. With the expressions given in the second columns of Tables 5 and 6, it is straightforward to calculate the magnetic moments of those baryons in free space as well as in symmetric nuclear matter.

For the transition magnetic moments in free space, $B = (\Sigma^0, \Sigma_c^+, \Sigma_b^0) \to B' = (\Lambda, \Lambda_c^+, \Lambda_b^0)$, denoted respectively by $\mu_{BB'} = (\mu_{\Sigma^0 \Lambda}, \mu_{\Sigma_c^+ \Lambda_c^+}, \mu_{\Sigma_b \Lambda_b})$, some discussions are in order. In a rigorous calculation in the MIT bag model [136], the bag radius difference for the initial and final baryons arises. This means that the same flavor spectator quark wave functions in the initial and final baryons are slightly different. Also, the integral upper limit is restricted to the common bag radius shown in Eq. (32), and the defects for the spectator quark wave function overlaps arise. However, we ignore these subtle points due to the MIT bag model, which are expected to give negligible effects (as shown later), and approximate each spectator quark wave function overlap to be unity. By these approximations, the moduli of the free space transition magnetic moments (the signs are not known) may be calculated by

$$|\mu_{\Sigma^0 \Lambda}| = |\mu_{\Sigma_c^+ \Lambda_c^+}| = |\mu_{\Sigma_b \Lambda_b}| = \frac{1}{\sqrt{3}} |\mu_u - \mu_d| \equiv \frac{1}{\sqrt{3}} |e_u \tilde{\eta}_u - e_d \tilde{\eta}_d|, \tag{31}$$

where $\tilde{\eta}_{u,d}$ in the last expression in Eq. (31) for $B = (\Sigma^0, \Sigma_c^+, \Sigma_b^0) \to B' = (\Lambda, \Lambda_c^+, \Lambda_b^0)$ are defined by

$$\tilde{\eta}_q \equiv (N_q^{B'} N_q^B) \int_0^{\min(R_{B'}, R_B)} dr\, r^2\, \frac{r}{3} \left[j_0(x_q' r/R_{B'})\, \beta_q^B\, j_1(x_q r/R_B) + \beta_q^{B'}\, j_1(x_q' r/R_{B'})\, j_0(x_q r/R_B) \right]. \tag{32}$$

The above expression may give rise to ambiguities due to the so-called MIT bag model artifact, similar to those discussed in the weak-interaction vector charge calculation: a naive

Table 5. Magnetic moments and transition magnetic moments in free space and in symmetric nuclear matter calculated with Set I (Table 1). The free space results are given in the third column in the nuclear magneton, $e/2m_N$ (e the positron charge and m_N the free nucleon mass, 939 MeV), with experimental data from Ref. [139] where it exists (fourth column), while the in-medium to free space ratios, $\mu_B^*(\rho_B)/\mu_B$ ($\mu_B \equiv \mu_B(\rho_B = 0)$) and $|\mu_{BB'}^*(\rho_B)/\mu_{BB'}|$ ($\mu_{BB'} \equiv \mu_{BB'}(\rho_B = 0)$) for $\rho_B = (\rho_0, 2\rho_0, 3\rho_0)$ with $\rho_0 = 0.15\,\mathrm{fm}^{-3}$ are given in the fifth, sixth, and seventh columns. The central values and errors for the free nucleon magnetic moments are shown with rounding in the table, but the correct values are shown in the table footnotes. The expressions in the second column are calculated using the flavor–spin wave functions with the "1–2 quark order" for the baryon $B(q_1, q_2, q_3)$, i.e. the quarks q_1 and q_2 are taken to be the closest in mass [106], which applies to the $\Xi_{c,b}$ baryons below.

$B(q_1, q_2, q_3)$	μ_B	μ_B	Experiment	$\frac{\mu_B^*(\rho_0)}{\mu_B}$	$\frac{\mu_B^*(2\rho_0)}{\mu_B}$	$\frac{\mu_B^*(3\rho_0)}{\mu_B}$
$p(uud)$	$(4\mu_u - \mu_d)/3$	1.535	2.793 ± 0.000^a	1.077	1.103	1.111
$n(ddu)$	$(4\mu_d - \mu_u)/3$	-1.023	-1.913 ± 0.000^b	1.077	1.103	1.111
$\Lambda(uds)$	μ_s	-0.429	-0.613 ± 0.004	0.997	0.991	0.985
$\Sigma^+(uus)$	$(4\mu_u - \mu_s)/3$	1.557	2.458 ± 0.010	1.086	1.133	1.162
$\Sigma^0(uds)$	$(2\mu_u + 2\mu_d - \mu_s)/3$	0.499		1.067	1.102	1.123
$\Sigma^-(dds)$	$(4\mu_d - \mu_s)/3$	-0.560	-1.160 ± 0.025	1.121	1.189	1.231
$\Xi^0(ssu)$	$(4\mu_s - \mu_u)/3$	-0.929	-1.250 ± 0.014	1.035	1.055	1.067
$\Xi^-(ssd)$	$(4\mu_s - \mu_d)/3$	-0.405	-0.6507 ± 0.0025	0.956	0.927	0.907
$\Delta^{++}(uuu)$	$3\mu_u$	3.341	3.7–9.8	1.099	1.151	1.181
$\Delta^+(uud)$	$2\mu_u + \mu_d$	1.671	$2.7^{+1.0\,c}_{-1.3}$	1.099	1.151	1.181
$\Delta^0(udd)$	$2\mu_d + \mu_u$	0	(SU(2) symmetry)	–	–	–
$\Delta^-(ddd)$	$3\mu_d$	-1.671		1.099	1.151	1.181
$\Sigma^{*+}(uus)$	$2\mu_u + \mu_s$	1.781		1.128	1.201	1.246
$\Sigma^{*0}(uds)$	$\mu_u + \mu_d + \mu_s$	0.102		1.571	1.906	2.120
$\Sigma^{*-}(dds)$	$2\mu_d + \mu_s$	-1.577		1.071	1.110	1.133
$\Xi^{*0}(ssu)$	$2\mu_s + \mu_u$	0.203		1.576	1.924	2.154
$\Xi^{*-}(ssd)$	$2\mu_s + \mu_d$	-1.473		1.038	1.060	1.073
$\Lambda_c^+(udc)$	μ_c	0.423		0.999	0.998	0.996
$\Sigma_c^{++}(uuc)$	$(4\mu_u - \mu_c)/3$	1.378		1.115	1.179	1.219
$\Sigma_c^+(udc)$	$(2\mu_u + 2\mu_d - \mu_c)/3$	0.238		1.166	1.261	1.319
$\Sigma_c^0(ddc)$	$(4\mu_d - \mu_c)/3$	-0.903		1.087	1.136	1.167
$\Xi_c^+(usc)$	μ_c	0.424		1.000	0.999	0.998
$\Xi_c^0(dsc)$	μ_c	0.424		1.000	0.999	0.998
$\Lambda_b^0(udb)$	μ_b	-0.073		1.000	1.000	1.000
$\Sigma_b^+(uub)$	$(4\mu_u - \mu_b)/3$	1.675		1.111	1.175	1.214
$\Sigma_b^0(udb)$	$(2\mu_u + 2\mu_d - \mu_b)/3$	0.437		1.107	1.167	1.205
$\Sigma_b^-(ddb)$	$(4\mu_d - \mu_b)/3$	-0.801		1.117	1.183	1.224
$\Xi_b^0(usb)$	μ_b	-0.073		1.000	1.000	1.000
$\Xi_b^-(dsb)$	μ_b	-0.073		1.000	1.000	1.000
Transition	$|\mu_{BB'}|$	$|\mu_{BB'}|$		$\frac{\mu_{BB'}^*(\rho_0)}{\mu_{BB'}}$	$\frac{\mu_{BB'}^*(2\rho_0)}{\mu_{BB'}}$	$\frac{\mu_{BB'}^*(3\rho_0)}{\mu_{BB'}}$
$\Sigma^0 \to \Lambda$	$|(\mu_u - \mu_d)/\sqrt{3}|$	0.868	1.61 ± 0.08	1.085	1.129	1.154
$\Sigma_c^+ \to \Lambda_c^+$	$|(\mu_u - \mu_d)/\sqrt{3}|$	0.899		1.086	1.128	1.151
$\Sigma_b^0 \to \Lambda_b^0$	$|(\mu_u - \mu_d)/\sqrt{3}|$	0.983		1.095	1.143	1.169

Notes. $^a\mu_p^{\mathrm{Experiment}} = 2.7928473446 \pm 0.0000000008$,
$^b\mu_n^{\mathrm{Experiment}} = -1.9130427 \pm 0.0000005$.
^{c} Theoretical uncertainties are not included [139].

integration over the common bag radius leads to a violation of the Ademoll–Gatto theorem [143] as discussed in Ref. [144]. Some discussions on this issue will be given later.

In the third columns in Tables 5 and 6 we give the free space magnetic moments and transition magnetic moments calculated with Set I (Table 1) and Set II (Table 2) respectively. The experimental data are also given in the fourth columns, but the values and errors for the nucleons are shown with rounding in the tables; the precise data are given in the footnotes of each table. As already mentioned, the calculated magnitude of the octet baryon magnetic moments in free space do not reproduce the data well. Our focus in this study is on their density dependence relative to the free space ones, which can still give some relevant and useful information. To

Table 6. As Table 5, but the results are calculated with the different current quark mass values for the strange and bottom quarks of Set II (Table 2).

$B(q_1, q_2, q_3)$	μ_B	μ_B	Experiment	$\frac{\mu_B^*(\rho_0)}{\mu_B}$	$\frac{\mu_B^*(2\rho_0)}{\mu_B}$	$\frac{\mu_B^*(3\rho_0)}{\mu_B}$
$p(uud)$	$(4\mu_u - \mu_d)/3$	1.535	2.793 ± 0.000^a	1.077	1.103	1.111
$n(ddu)$	$(4\mu_d - \mu_u)/3$	-1.023	-1.913 ± 0.000^b	1.077	1.103	1.111
$\Lambda(uds)$	μ_s	-0.500	-0.613 ± 0.004	0.996	0.990	0.983
$\Sigma^+(uus)$	$(4\mu_u - \mu_s)/3$	1.628	2.458 ± 0.010	1.088	1.137	1.166
$\Sigma^0(uds)$	$(2\mu_u + 2\mu_d - \mu_s)/3$	0.535		1.066	1.103	1.123
$\Sigma^-(dds)$	$(4\mu_d - \mu_s)/3$	-0.559	-1.160 ± 0.025	1.113	1.204	1.250
$\Xi^0(ssu)$	$(4\mu_s - \mu_u)/3$	-1.068	-1.250 ± 0.014	1.035	1.054	1.066
$\Xi^-(ssd)$	$(4\mu_s - \mu_d)/3$	-0.509	-0.6507 ± 0.0025	0.960	0.934	0.915
$\Delta^{++}(uuu)$	$3\mu_u$	3.341	3.7–9.8	1.099	1.151	1.181
$\Delta^+(uud)$	$2\mu_u + \mu_d$	1.671	$2.7^{+1.0}_{-1.3}{}^c$	1.099	1.151	1.181
$\Delta^0(udd)$	$2\mu_d + \mu_u$	0	(SU(2) symmetry)	$-$	$-$	$-$
$\Delta^-(ddd)$	$3\mu_d$	-1.671		1.099	1.151	1.181
$\Sigma^{*+}(uus)$	$2\mu_u + \mu_s$	1.767		1.137	1.216	1.265
$\Sigma^{*0}(uds)$	$\mu_u + \mu_d + \mu_s$	0.040		2.558	3.486	4.085
$\Sigma^{*-}(dds)$	$2\mu_d + \mu_s$	-1.687		1.070	1.109	1.132
$\Xi^{*0}(ssu)$	$2\mu_s + \mu_u$	0.083		2.566	3.515	4.139
$\Xi^{*-}(ssd)$	$2\mu_s + \mu_d$	-1.686		1.037	1.058	1.071
$\Lambda_c^+(udc)$	μ_c	0.423		0.999	0.998	0.996
$\Sigma_c^{++}(uuc)$	$(4\mu_u - \mu_c)/3$	1.378		1.115	1.179	1.219
$\Sigma_c^+(udc)$	$(2\mu_u + 2\mu_d - \mu_c)/3$	0.238		1.166	1.261	1.319
$\Sigma_c^0(ddc)$	$(4\mu_d - \mu_c)/3$	-0.903		1.087	1.136	1.167
$\Xi_c^+(usc)$	μ_c	0.426		1.000	0.999	0.998
$\Xi_c^0(dsc)$	μ_c	0.426		1.000	0.999	0.998
$\Lambda_b^0(udb)$	μ_b	-0.074		1.000	1.000	1.000
$\Sigma_b^+(uub)$	$(4\mu_u - \mu_b)/3$	1.681		1.112	1.175	1.215
$\Sigma_b^0(udb)$	$(2\mu_u + 2\mu_d - \mu_b)/3$	0.439		1.107	1.168	1.206
$\Sigma_b^-(ddb)$	$(4\mu_d - \mu_b)/3$	-0.804		1.117	1.184	1.225
$\Xi_b^0(usb)$	μ_b	-0.074		1.000	1.000	1.000
$\Xi_b^-(dsb)$	μ_b	-0.074		1.000	1.000	1.000
Transition	$|\mu_{BB'}|$	$|\mu_{BB'}|$		$\frac{\mu_{BB'}^*(\rho_0)}{\mu_{BB'}}$	$\frac{\mu_{BB'}^*(2\rho_0)}{\mu_{BB'}}$	$\frac{\mu_{BB'}^*(3\rho_0)}{\mu_{BB'}}$
$\Sigma^0 \to \Lambda$	$|(\mu_u - \mu_d)/\sqrt{3}|$	0.901	1.61 ± 0.08	1.089	1.136	1.163
$\Sigma_c^+ \to \Lambda_c^+$	$|(\mu_u - \mu_d)/\sqrt{3}|$	0.899		1.086	1.128	1.151
$\Sigma_b^0 \to \Lambda_b^0$	$|(\mu_u - \mu_d)/\sqrt{3}|$	0.988		1.095	1.144	1.170

Notes. $^a\mu_p^{\text{Experiment}} = 2.7928473446 \pm 0.0000000008$.
$^b\mu_n^{\text{Experiment}} = -1.9130427 \pm 0.0000005$.
^{c}Theoretical uncertainties are not included [139].

give some idea on the free-space baryon magnetic moments calculated in the present approach, we compare in Table 7 the free-space baryon magnetic moments obtained by various models and lattice QCD simulations.

Recall that the in-medium to free proton EMFF ratios predicted by the QMC model reproduce well the extracted proton EMFF super ratio $[G_{\rm E}^p/G_{\rm M}^p(^4{\rm He})]/[G_{\rm E}^p/G_{\rm M}^p(^1{\rm H})]$ from the $^4{\rm He}(\vec{e}, e'\vec{p})^3{\rm H}$ reaction measured at Jefferson Laboratory [125–127]. The ratios of the in-medium to free space magnetic moments are given for three baryon densities, ρ_0, $2\rho_0$, and $3\rho_0$, in the fifth, sixth, and seventh columns in Tables 5 and 6 for Sets I and II respectively.

Here, we focus on the in-medium nucleon magnetic moments. As already mentioned, the constraint for the allowed change (swelling) of the in-medium nucleon size, thus for the in-medium nucleon bag radii and magnetic moments, is allowed to increase no more than 17.1% at ρ_0, if we properly take the y-scaling analysis results. The present QMC model results give a 7.7% enhancement of the nucleon magnetic moments at ρ_0, well within the constraint.

One can notice that most of the ratios become larger as the baryon density increases, except for Λ, Ξ^-, Λ_c^+, Λ_b, $\Xi_c^{+,0}$, and $\Xi_b^{0,-}$. In particular, the large enhancement for the Σ^{*0} and Ξ^{*0}

Table 7. Comparison of the free-space baryon magnetic moments (in the nuclear magneton) by various models and lattice QCD simulations [145–147] that are different from the MIT bag model, focusing on heavier baryons since the data for the octet baryons exist, where the model uncertainties (errors) are not given below even when quoted in some references. For some experimental values, see Tables 5 and 6.

$B(q_1, q_2, q_3)$	Set I	Set II	[102,103]	[111]	[113]	[114]	[115]	[116]	[145,146]	[147]
$p(uud)$	1.535	1.535	2.56	–	–	–	2.8732	2.886	2.3	3.04
$n(ddu)$	−1.023	−1.023	−1.93	–	–	–	−1.9154	−1.924	−1.3	−1.84
$\Lambda(uds)$	−0.429	−0.500	−0.55	–	–	–	−0.5512	−0.580	−0.40	−0.70
$\Sigma^+(uus)$	1.557	1.628	2.60	–	–	–	2.7377	2.758	1.9	2.87
$\Sigma^0(uds)$	0.499	0.535	−1.48	–	–	–	0.8222	0.834	0.54	0.76
$\Sigma^-(dds)$	−0.560	−0.559	−1.26	–	–	–	−1.0932	−1.089	−0.87	−1.48
$\Xi^0(ssu)$	−0.929	−1.068	−1.32	–	–	–	−1.3734	−1.414	−0.95	−1.37
$\Xi^-(ssd)$	−0.405	−0.509	−0.57	–	–	–	−0.4157	−0.452	−0.41	−0.82
$\Delta^{++}(uuu)$	3.341	3.341	5.267	–	–	–	–	–	4.91	5.24
$\Delta^+(uud)$	1.671	1.671	2.430	–	–	–	–	–	2.46	0.97
$\Delta^0(udd)$	0	0	−0.408	–	–	–	–	–	0.00	−0.035
$\Delta^-(ddd)$	−1.671	−1.671	−3.245	–	–	–	–	–	−2.46	−2.98
$\Sigma^{*+}(uus)$	1.781	1.767	3.208	–	–	–	–	–	2.55	1.27
$\Sigma^{*0}(uds)$	0.102	0.040	0.188	–	–	–	–	–	0.27	0.33
$\Sigma^{*-}(dds)$	−1.577	−1.687	−2.105	–	–	–	–	–	−2.02	−1.88
$\Xi^{*0}(ssu)$	0.203	0.083	0.508	–	–	–	–	–	0.46	0.16
$\Xi^{*-}(ssd)$	−1.473	−1.686	−1.805	–	–	–	–	–	−1.68	−0.62
$\Lambda_c^+(udc)$	0.423	0.423	–	–	0.42	0.385	0.341	0.352	–	–
$\Sigma_c^{++}(uuc)$	1.378	1.378	–	2.4	1.76	2.279	2.44	2.448	–	–
$\Sigma_c^+(udc)$	0.238	0.238	–	0.5	0.36	0.501	0.525	0.524	–	–
$\Sigma_c^0(ddc)$	−0.903	−0.903	–	−1.5	−1.04	−1.015	−1.391	−1.400	–	–
$\Xi_c^+(usc)$	0.424	0.426	–	0.8	0.41	0.711	0.796	0.779	–	–
$\Xi_c^0(dsc)$	0.424	0.426	–	−1.2	0.39	−0.966	−1.12	−1.145	–	–
$\Lambda_b^0(udb)$	−0.073	−0.074	–	–	−0.06	−0.064	–	–	–	–
$\Sigma_b^+(uub)$	1.675	1.681	–	2.4	2.07	2.229	2.575	2.586	–	–
$\Sigma_b^0(udb)$	0.437	0.439	–	0.6	0.53	0.592	0.659	0.662	–	–
$\Sigma_b^-(ddb)$	−0.801	−0.804	–	−1.3	−1.01	−1.047	−1.256	−1.261	–	–
$\Xi_b^0(usb)$	−0.073	−0.074	–	0.7	−0.06	0.766	0.93	0.917	–	–
$\Xi_b^-(dsb)$	−0.073	−0.074	–	−1.2	−0.06	−0.902	−0.985	−1.006	–	–

may be noted in both Sets I and II. This enhancement is due to the small magnitudes of these magnetic moments in free space, as can been seen in Tables 5 and 6. Between the corresponding results given in Tables 5 and 6, one can also see the effect of the different strange quark mass values, respectively $m_s = 250$ MeV and $m_s = 93$ MeV. The absolute value of the strange quark magnetic moment $|\mu_s|$ becomes smaller, $0.429 \to 0.275$, as the m_s value changes $250 \to 93$ MeV. Then, all changes involving the strange quark magnetic moment can be understood in Table 6 as follows. Namely, the corresponding magnetic moments in Table 6 are less influenced by the strange quark magnetic moment $\mu_s < 0$ than those in Table 5. On the other hand, the use of $m_b = 4200$ MeV or $m_b = 4180$ MeV gives negligible difference.

The tiny decreases (or no changes up to the digits shown) observed for the magnetic moments of Λ, Ξ^-, Λ_c^+, Λ_b, $\Xi_c^{+,0}$, and $\Xi_b^{0,-}$ as the baryon density increases can be understood as follows. Their total magnetic moments are μ_s, μ_c, or μ_b for the Λ and the corresponding Λ-like baryons, or $(4\mu_s - \mu_{u,d})/3$ for $\Xi^{0,-}$. In the QMC model, the s, c, and b quarks do not couple the mean fields σ or ω. Thus, their wave functions are not directly modified as the first-order interactions of σ and ω mean fields. However, the mean fields, in particular the σ field, couple to the light quarks u and d in these baryons, and the effective masses of these baryons decrease (or they get the attractive Lorentz scalar potentials) as the baryon density increases. Accordingly, the bag radii of these baryons decrease very slightly as the baryon density increases [21] as a consequence of the simultaneous mass stability condition, Eq. (13). Since the baryon (quark)
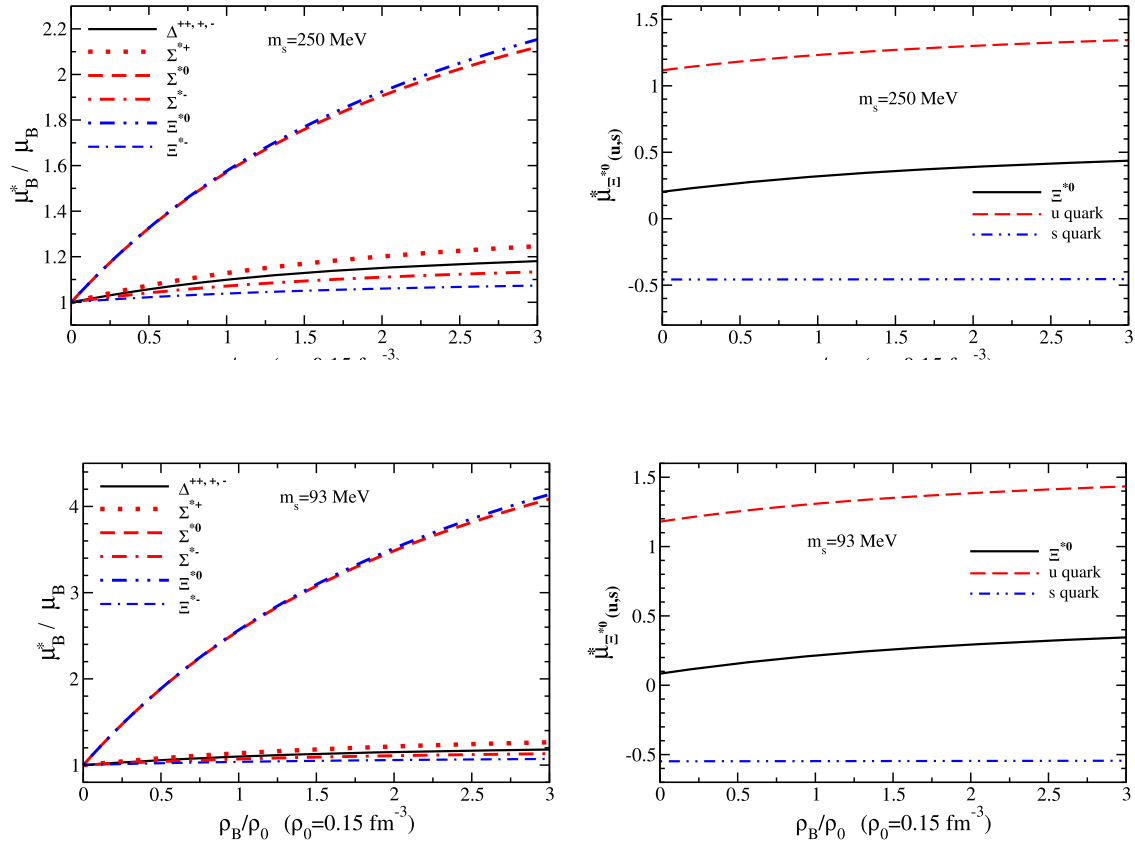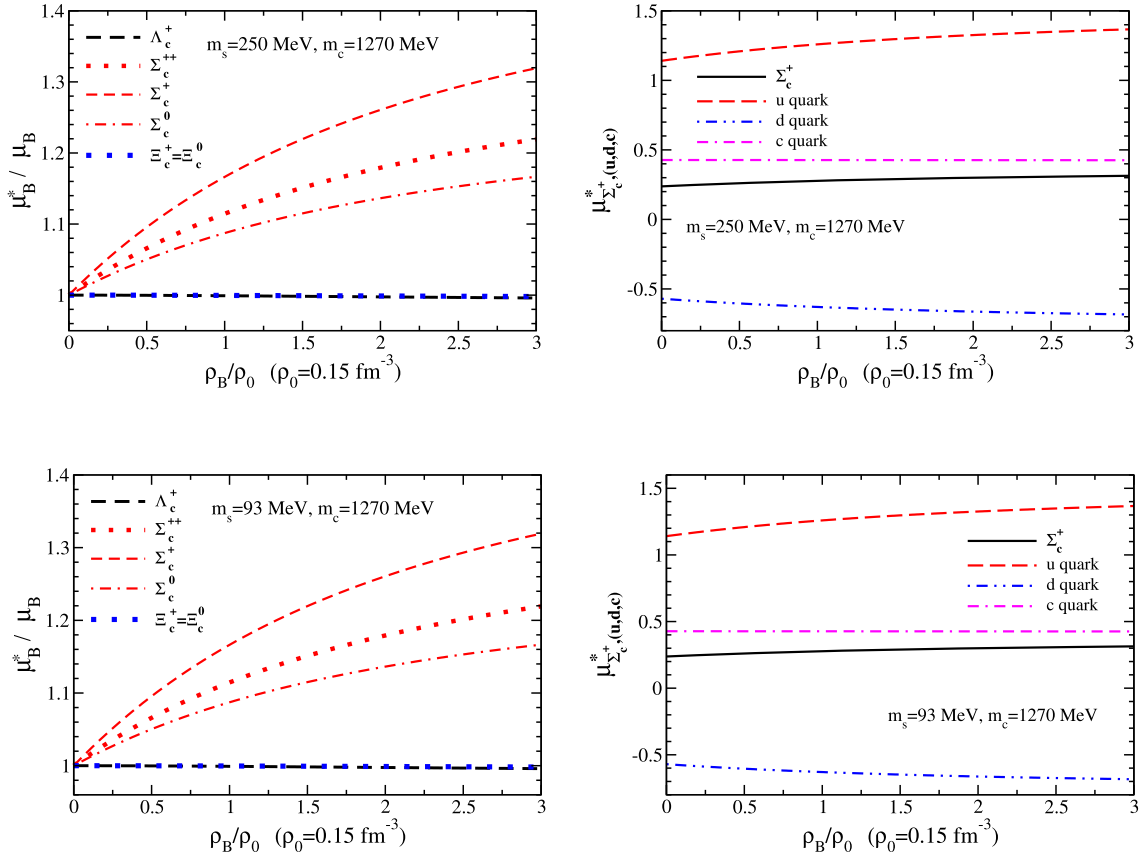
Fig. 4. Density dependence of the octet baryon magnetic moment ratios, the in-medium to free space (left panel), and the bare Σ^- magnetic moment, which has the largest medium modification in the left panel, and the corresponding d and s quark magnetic moments (right panel), respectively calculated for Set I (upper panel) and Set II (lower panel).

magnetic moment is roughly proportional to the bag radius, and the wave functions of the s, c, and b quarks are not modified as the first order, the s, c, and b quark magnetic moments are slightly modified as a second-order effect of the bag radius change, and thus the in-medium quark magnetic moments $\mu^*_{s,c,b}$ decrease very slightly due to the bag radius decrease. The $\Xi^{0,-}$ cases are similar, because μ^*_s dominates. Thus, the magnetic moments of Λ, Ξ^-, Λ^+_c, Λ_b, $\Xi^{+,0}_c$, and $\Xi^{0,-}_b$ decrease very slightly as the baryon density increases.

To see this more easily, we show the density dependence of the magnetic moments of the octet baryons in Fig. 4, decuplet baryons in Fig. 5, low-lying charmed baryons in Fig. 6, low-lying bottom baryons in Fig. 7, and the transition magnetic moments in Fig. 8, calculated for Sets I and II. In each figure the ratios of the in-medium to free space are shown in the left panel for both Set I (upper left) and Set II (lower left), while in the right panel the bare density dependence is shown for the magnetic moment that has the largest medium modification among all in the left panel, as well as the corresponding quark contributions for Set I (upper right) and Set II (lower right).

First, we discuss the magnetic moments of the octet baryons shown in Fig. 4. As is known, the MIT bag model underestimates the octet baryon magnetic moments in free space [151,152], and the analytic expression for the magnetic moment is roughly proportional to the bag radius. (For example, see Ref. [153, Table 7.1] for the bag radius dependence on the numerically obtained

Fig. 5. Density dependence of the decuplet baryon magnetic moment ratios, the in-medium to free space (left panel), and the bare Ξ^{*0} magnetic moment, which has the largest medium modification in the left panel, and the corresponding u and s quark magnetic moments (right panel), respectively calculated for Set I (upper panel) and Set II (lower panel).

octet baryon magnetic moments.) Thus, we estimate the medium modifications of magnetic moments by taking the ratios of the in-medium to free space magnetic moments. The calculated density dependence of the ratios (left panel) is quite different from that of the MQMC model shown in Ref. [100]. It is desirable to properly take into account the constraint for the allowed maximum change derived from the y-scaling data analysis.

In the right panel we show the Σ^- magnetic moment, which has the largest medium modification among all in the left panel, as well as the corresponding quark contributions. One can see that the s quark magnetic moment is only slightly modified in medium, showing a small linear increase as the density increases. This very small density dependence is expected, since the s quark does not couple to any meson fields in the present model, and the modification comes from the change in the bag radius R_Σ^*.

Next, we show the decuplet baryon magnetic moments in Fig. 5. The Σ^{*0} and Ξ^{*0} magnetic moments have large enhancements as the baryon density increases for both Sets I and II. This enhancement, as already mentioned, is due to their small magnitudes in free space.

As for the charm sector baryon magnetic moments shown in Fig. 6, one can easily notice that the medium modification of the Σ_c^+ magnetic moment is the largest in the left panel, while those of Λ_c^+ and $\Xi_c^{+,0}$ are negligibly modified (tiny decrease). The Σ_c^+ magnetic moment is enhanced in the ratio by the small magnitude of the free space magnetic moment as shown in Tables 5
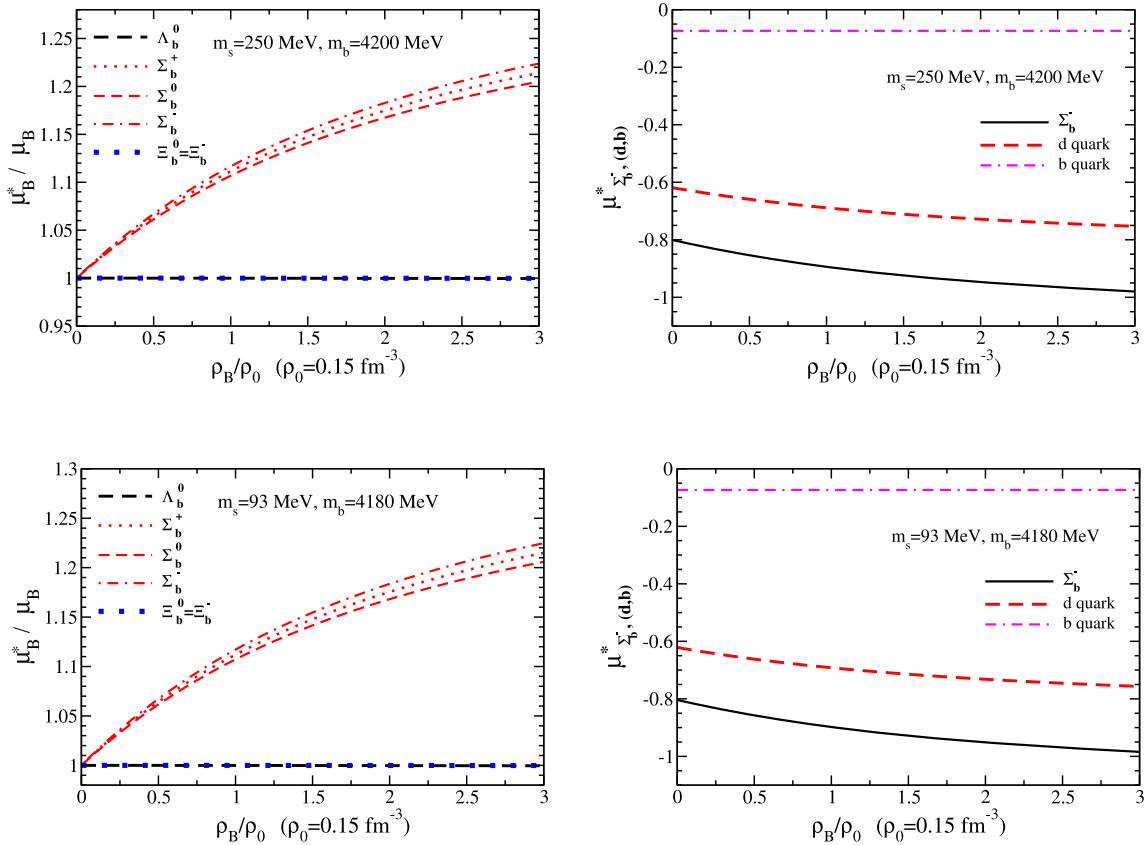
Fig. 6. Density dependence of the charm baryon magnetic moment ratios, the in-medium to free space (left panel), and the bare Σ_c^+ magnetic moment, which has the largest medium modification in the left panel, and the corresponding u, s, and c quark magnetic moments (right panel), respectively calculated for Set I (upper panel) and Set II (lower panel).

and 6. As can be confirmed for the Σ_c^+ in the right panel, the increase of the u quark magnetic moment enhances the ratio.

For the bottom baryon magnetic moments shown in Fig. 7, the $\Sigma_b^{\pm,0}$ magnetic moments show large medium modifications in the left panel. Differently from the case of $\Sigma_c^{++,+,0}$, the magnitudes of the free space magnetic moments do not reflect the enhancement of the ratio of the $\Sigma_b^{\pm,0}$ magnetic moments. Similar to the charm sector, the Λ_b and $\Xi_b^{+,0}$ are negligibly modified (tiny decrease) as expected.

Finally, we show in Fig. 8 the transition magnetic moments for $B = (\Sigma^0, \Sigma_c^+, \Sigma_b^0) \to B' = (\Lambda, \Lambda_c^+, \Lambda_b^0)$, calculated for Set I (upper panel) and Set II (lower panel). The density dependence of the in-medium to free space ratios is shown in the left panel, while the moduli of the bare values are shown in the right panel. The density dependence seems to be similar for all three cases in the left panel, but the $\Sigma_b^0 \to \Lambda_b$ case shows a larger enhancement for both Set I and Set II. The larger medium modification of $|\mu_{\Sigma_b^0 \Lambda_b^0}|$, which can be seen in the left panel, may be attributed to the larger bag radii for the $(\Sigma_b^0 \to \Lambda_b^0)$, or the larger integral upper limit (common bag radius) $R_{\Lambda_b}^*$ than those of R_Λ^* for $(\Sigma^0 \to \Lambda)$ and $R_{\Lambda_c^+}^*$ for $(\Sigma_c^+ \to \Lambda_c^+)$. In addition, the effect due to the different m_s values can be seen in the enhancement of the $\Sigma^0 \to \Lambda$ transition magnetic moment in the bottom right. In this case, the results show that the $m_s = 93$ MeV (Set II) yields larger bag radii for the Σ and Λ than those corresponding to $m_s = 250$ MeV

Fig. 7. Density dependence of the bottom baryon magnetic moment ratios, the in-medium to free space (left panel), and the bare Σ_b^- magnetic moment, which has the largest medium modification in the left panel, and the corresponding u, s, and b quark magnetic moments (right panel), respectively calculated for Set I (upper panel) and Set II (lower panel).

(Set I), giving the larger transition magnetic moment, since the transition magnetic moments are also roughly proportional to the bag radii of the initial and final baryons, or common bag radius. Since this feature may be associated with the MIT bag model artifact, we should focus on the ratios, the in-medium to free space shown in the left panel, as will be discussed next. As already mentioned, ratios are also used to extract the useful and meaningful experimental data to reduce ambiguities.

Let us discuss here some aspects of partial restoration of dynamical chiral symmetry (PRDCS) on the in-medium magnetic moments obtained. As already mentioned, dynamical chiral symmetry (DCS) and its partial restoration concern the light quarks—the faster reductions of light quark condensates. The reductions result in a decrease of the (effective) masses of baryons (hadrons) which contain light quarks. Thus, the largest effect is expected to appear in the nucleon magnetic moments, likewise the mass reductions of the nucleons are the largest among the baryons treated in this study, since nucleons are composed of purely light quarks. Or, the magnitude of mass reduction (attractive Lorentz scalar potential) appears in proportion to the number of light quarks in the baryon, namely from the larger to smaller order, N, $\Lambda_{s,c,b} \simeq \Sigma_{s,c,b}$, and $\Xi_{s,c,b}$ ($\Lambda_s \equiv \Lambda$). For the case of the baryon magnetic moments, though, the story is a bit different, since the $\Lambda_{s,c,b}$ magnetic moments are respectively equal to $\mu_{s,c,b}$ without the light quark contributions. Note that, the effects of PRDCS are for the "net" modifications of the
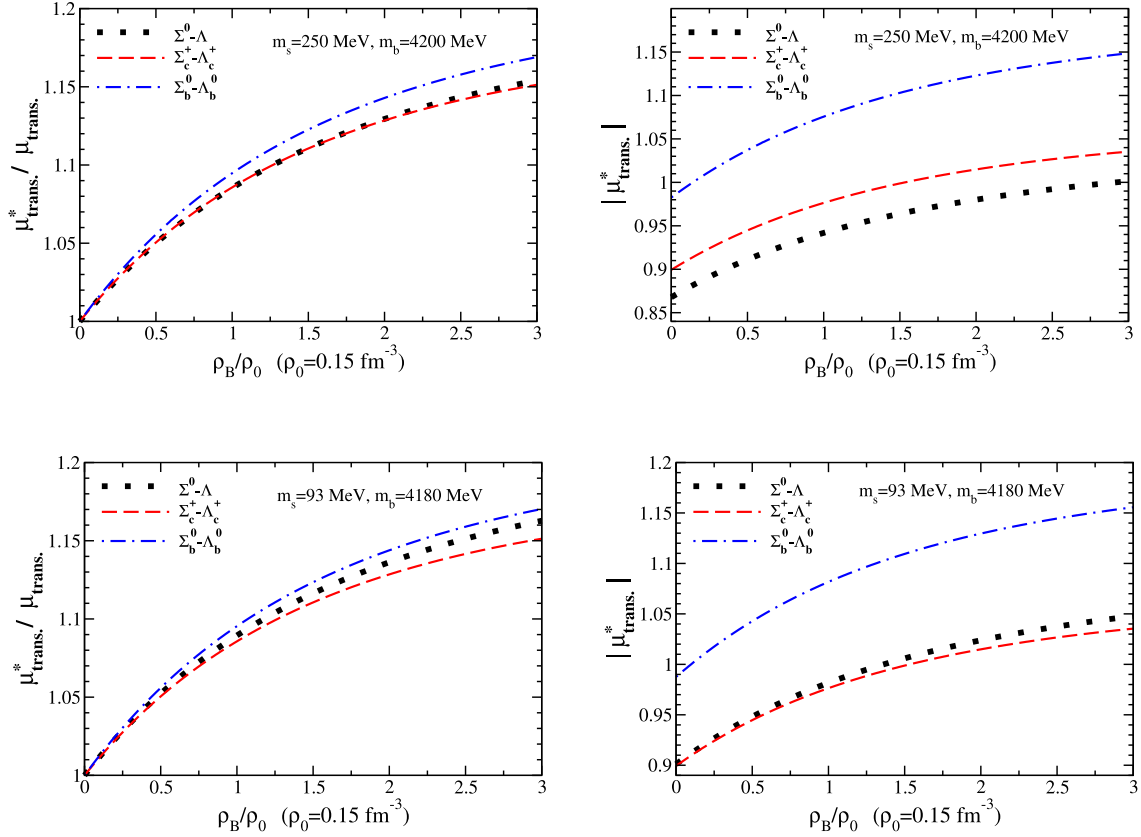
Fig. 8. Density dependence of the transition magnetic moment ratios, the in-medium to free space (left panel), and the moduli of the bare values in medium (right panel), respectively calculated for Set I (upper panel) and Set II (lower panel).

light quark magnetic moments μ_u and μ_d. For the transition magnetic moments, since all three transitions treated in this study are proportional to $|(\mu_u - \mu_d)/\sqrt{3}|$, the transition magnetic moments reflect directly the PRDCS. In the ratios shown in Figs. 4–8, the modifications of the μ_u and μ_d are modulated by the other contributions from s, c, and b quark magnetic moments, respectively $\mu_{s,c,b}$, for the sum for each baryon magnetic moment except for those of $\Lambda_{s,c,b}$. In addition, a small but non-negligible modification of the in-medium bag radius of each baryon influences the in-medium magnetic moment by a small amount. (In the MIT bag model the magnetic moment of a baryon is roughly proportional to the bag radius.) Although the results shown in Figs. 4–8 contain these mixed effects in the ratios, the clear conclusion is that the light quark in-medium to free magnetic moment ratios become enhanced to be $|\mu^*_{u,d}/\mu_{u,d}| > 1$, and these inequalities are valid for all the relevant baryons in medium, although for $\Lambda_{s,c,b}$ and $\Xi_{c,b}$ they do not explicitly contribute and affect the results. The magnetic moments of $\mu_{s,c,b}$ are not modified in the first-order effects of PRDCS in the QMC model. These features can be clearly seen from the right panels in Figs. 4–8.

Next, we discuss the ratios of the in-medium to free space transition magnetic moments, since the ratios are expected to reduce the possible ambiguities originating from the MIT bag model artifact as follows. Let us denote the true values in medium as $\mu^{*\text{true}}_{BB'}(\rho_B)$ and in free space as $\mu^{\text{true}}_{BB'}(0)$, respectively, and the corresponding errors by $\epsilon^*(\rho_B)$ and $\epsilon(0)$. Then, the ratio of the

in-medium to free space can be estimated by

$$\frac{\mu^*_{BB'}(\rho_B)}{\mu_{BB'}(0)} = \frac{\mu^{*\mathrm{true}}_{BB'}(\rho_B)(1 \pm \epsilon^*(\rho_B))}{\mu^{\mathrm{true}}_{BB'}(0)(1 \pm \epsilon(0))}$$

$$\simeq \frac{\mu^{*\mathrm{true}}_{BB'}(\rho_B)}{\mu^{\mathrm{true}}_{BB'}(0)}(1 \pm \epsilon^*(\rho_B) \mp \epsilon(0)) = \frac{\mu^{*\mathrm{true}}_{BB'}(\rho_B)}{\mu^{\mathrm{true}}_{BB'}(0)}[1 \pm (\epsilon^*(\rho_B) - \epsilon(0))], \qquad (33)$$

where $0 < \epsilon^*(\rho_B), \epsilon(0) \ll 1$ are assumed. The signs in front of them in the first line in Eq. (33) are expected to be the same, since $\epsilon^*(\rho_B)$ varies smoothly as $\rho_B \to 0$, and $\epsilon^*(\rho_B) \to \epsilon(0)$ to make the ratio unity. Then, $|(\epsilon^*(\rho_B) - \epsilon(0))|$ becomes smaller in Eq. (33).

To get a better idea of the bag radius difference, we estimate the differences in free space and at ρ_0 [21] with the Set I and Set II results, and obtain

$$\left(\frac{R_B(0) - R_{B'}(0)}{R_{B'}(0)}, \frac{R_B^*(\rho_0) - R_{B'}^*(\rho_0)}{R_{B'}^*(\rho_0)} \right) < (0.045, 0.045), \qquad (34)$$

where the inequality holds for all three cases, $B = (\Sigma^0, \Sigma_c^+, \Sigma_b^0) \to B' = (\Lambda, \Lambda_c^+, \Lambda_b^0)$ with $R_B(0) - R_{B'}(0) > 0$ and $R_B^*(\rho_0) - R_{B'}^*(\rho_0) > 0$, for both sets (Tables 1 and 2). Furthermore, since the bag model result for the diagonal magnetic moment μ_B (μ_B^*) is roughly proportional to the bag radius R_B (and R_B^*) [151], we can expect the size of the ambiguity to be of the same order as in Eq. (34).

In fact, the octet baryon magnetic moments and transition magnetic moments were studied in the U(3) symmetry model [148] (equivalent to the SU(3) symmetry model of Refs. [149,150] for this case), by including up to the first order of mass splitting interaction. Then, the following relations were obtained:

$$\mu_{\Sigma^0} = \frac{1}{2}[\mu_{\Sigma^+} + \mu_{\Sigma^-}], \qquad (35)$$

$$\mu_{\Sigma^0 \Lambda} = \mu_{\Lambda \Sigma^0} = \frac{1}{2\sqrt{3}}[\mu_{\Sigma^0} + 3\mu_\Lambda - 2\mu_{\Xi^0} - 2\mu_n]. \qquad (36)$$

We examine the above relations in the present results of the MIT bag model in free space. For Eq. (35), we get the left-hand side (LHS) and right-hand side (RHS) values of (LHS, RHS) = (0.499, 0.499) [(0.457,0.457)] using the values in Table 5 (Set I) [Table 6 (Set II)], while for Eq. (36) we get (LHS, RHS) = (0.868, 0.900) [(0.901,0.914)]. For the latter, the deviation may be estimated as $(0.900 - 0.868)/0.868 = 0.037$ [$(0.914 - 0.901)/0.901 = 0.014$]. On the other hand, using the experimental data for the octet baryon magnetic moments and $|\mu^{\mathrm{Expt.}}_{\Sigma^0 \to \Lambda}| = 1.61$ [139] with $\mu_{\Sigma^0} \equiv (1/2)[\mu^{\mathrm{Experiment}}_{\Sigma^+} + \mu^{\mathrm{Experiment}}_{\Sigma^-}]$, we get (LHS, RHS) = (1.61, 1.483) for Eq. (36). The deviation is estimated by $(1.61 - 1.483)/1.483 = 0.086$. Thus, including the SU(3) symmetry-breaking mass splitting interaction up to the first order, the deviation from the relation is larger when we use the experimental results than using the MIT bag model results for both Sets I and II. Based on these estimates, the ambiguities arising from the possible MIT bag model artifact, such as the bag radius difference, are not expected to affect the estimated ratios for the transition magnetic moments within the present status of the experimental precision.

To make the analysis complete, we also study the Coleman–Glashow relations [154] that were derived in a unitary symmetry scheme by defining the ratios R_i ($i = 1, ..., 8$):

$$\mu_{\Sigma^+} = \mu_p \qquad\qquad \to R_1 \equiv \left| \frac{\mu_{\Sigma^+} - \mu_p}{\mu_p} \right|, \qquad (37)$$

$$\mu_\Lambda = \frac{1}{2}\mu_n \qquad\qquad \to R_2 \equiv \left| \frac{\mu_\Lambda - \frac{1}{2}\mu_n}{\frac{1}{2}\mu_n} \right|, \qquad (38)$$

Table 8. The ratios R_i ($i = 1, \ldots, 8$) from Eqs. (37)–(44) calculated with Set I, Set II, and experimental data, corresponding to the Coleman–Glashow relations [154], and the ratios for experimental data, μ_B/μ_B(Experiment), where μ_{Σ^0}(Experiment) $= \frac{1}{2}[\mu_{\Sigma^+}$(Experiment) $+ \mu_{\Sigma^-}$(Experiment)] $= 0.649$ is used.

Ratio	Set I	Set II	Experiment
R_1	0.014	0.061	0.120
R_2	0.163	0.022	0.359
R_3	0.092	0.044	0.347
R_4	0.094	0.092	0.318
R_5	0.209	0.006	0.207
R_6	0.277	0.089	0.439
R_7	0.024	0.046	0.322
R_8	0.020	0.017	0.028
μ_p/μ_p(Experiment)	0.550	0.550	1
μ_n/μ_n(Experiment)	0.535	0.535	1
μ_Λ/μ_Λ(Experiment)	0.700	0.816	1
$\mu_{\Sigma^+}/\mu_{\Sigma^+}$(Experiment)	0.633	0.662	1
$\mu_{\Sigma^0}/\mu_{\Sigma^0}$(Experiment)	0.769	0.828	1
$\mu_{\Sigma^-}/\mu_{\Sigma^-}$(Experiment)	0.483	0.481	1
μ_{Ξ^0}/μ_{Ξ^0}(Experiment)	0.743	0.854	1
μ_{Ξ^-}/μ_{Ξ^-}(Experiment)	0.622	0.782	1

$$\mu_{\Xi^0} = \mu_n \qquad \rightarrow R_3 \equiv \left| \frac{\mu_{\Xi^0} - \mu_n}{\mu_n} \right|, \tag{39}$$

$$\mu_{\Sigma^-} = -[\mu_p + \mu_n] \qquad \rightarrow \quad R_4 \equiv \left| \frac{\mu_{\Sigma^-} + [\mu_p + \mu_n]}{-[\mu_p + \mu_n]} \right|, \tag{40}$$

$$\mu_{\Xi^-} = -[\mu_p + \mu_n] \qquad \rightarrow R_5 \equiv \left| \frac{\mu_{\Xi^-} + [\mu_p + \mu_n]}{-[\mu_p + \mu_n]} \right|, \tag{41}$$

$$\mu_{\Xi^-} = \mu_{\Sigma^-} \qquad \rightarrow R_6 \equiv \left| \frac{\mu_{\Xi^-} - \mu_{\Sigma^-}}{\mu_{\Sigma^-}} \right|, \tag{42}$$

$$\mu_{\Sigma^0} = -\frac{1}{2}\mu_n \qquad \rightarrow R_7 \equiv \left| \frac{\mu_{\Sigma^0} + \frac{1}{2}\mu_n}{-\frac{1}{2}\mu_n} \right|, \tag{43}$$

$$|\mu_{\Sigma^0\Lambda}| = \left| \frac{1}{2}\sqrt{3}\mu_n \right| \qquad \rightarrow R_8 \equiv \left| \frac{|\mu_{\Sigma^0\Lambda}| - \left| \frac{1}{2}\sqrt{3}\mu_n \right|}{\frac{1}{2}\sqrt{3}\mu_n} \right|. \tag{44}$$

In the above, R_i ($i = 1, \ldots, 8$) will be evaluated with the experimental data and the results from Sets I and II, where we have already analyzed the relation μ_{Σ^0}(Experiment) $= \frac{1}{2}[\mu_{\Sigma^+}$(Experiment) $+ \mu_{\Sigma^-}$(Experiment)] $= 0.649$ by Eq. (35), which is independent of the unitary symmetry scheme, and we will use this value as μ_{Σ^0}(Experiment) in this analysis. We also take into account the unknown sign in the experiment of $|\mu_{\Sigma^0\Lambda}|$. The obtained ratios R_i ($i = 1, \ldots, 8$) for Sets I and II and Experiment are given in Table 8. In addition, we give the ratios μ_B/μ_B(Experiment) for convenience.

The results for R_i ($i = 1, \ldots, 8$) given in Table 8 show that the Coleman–Glashow relations [154] are broken by up to about 45% in the data, and up to about 30% (70%) in the Set I (Set II) results. The Coleman–Glashow relations are not realized well in nature, as well as in

the MIT bag model results obtained for Sets I and II. In particular, the values for R_8 in Eq. (44) associated with $\mu_{\Sigma^0\Lambda}$ are respectively obtained as (Set I, Set II, Experiment) = (0.020, 0.017, 0.028), and the experimental data give a larger deviation from the Coleman–Glashow relation. Thus, the ambiguity due to the possible MIT bag model artifact (the bag radii difference, etc.) is not expected to significantly affect the conclusions for the transition magnetic moments in medium.

The estimated medium modifications of the magnetic moments and the transition magnetic moments at the nuclear matter saturation density (ρ_0) may not be directly reflected in the experimental results. In future experiments, although it is expected to be very difficult, if the charmed/bottom hypernuclei can be formed, for example, it might not be impossible to measure the magnetic moments of the bound charmed/bottom baryons for those treated in this study. For example, similarly to the proton knockout reaction used for extracting the bound proton electromagnetic form factor double ratios by a polarization transfer measurement, it might be possible to extract the charged charm/bottom baryon electromagnetic form factor double ratios at very small momentum transfer, where the charge form factor at zero momentum transfer gives the charge, and the information on the in-medium magnetic moment can be extracted. But, such possibilities are, at present, very remote and speculative.

However, the modifications in the higher-density region near $3\rho_0$ may affect some studies of heavy ion collisions, and the structure and reactions occuring in the inner cores of magnetars, neutron stars, and compact stars. In the cores of such high-density compact objects, in particular very high-density compact stars, one may expect the appearance of charm and bottom baryons, although no charm quark-matter star is expected to be stable [18–20], using the flat space-time equations of state (EOS). However, it has been discussed that the use of EOS computed in the curved space-time of neutron stars may yield higher central energy densities and masses—about 16.9% for an idealistic neutron star case—than when calculated using the flat-space EOS [155]. The authors state that the result favors resolving the "hyperon puzzle" of the neutron star. We would like to comment that, within the QMC model treatment, the possibility of resolving the "hyperon puzzle" due to the quark structure of nucleons and hyperons has been reported in Refs. [59–63]. It might be interesting to study the possibility of a charm quark-matter star as well as very high-density compact stars using the curved space-time EOS including the charm and bottom baryons to study whether or not such heavy baryons can indeed influence the structure. In addition, dominant charm hadron contributions to neutrino fluence in ultra high-energy neutrino production by newborn magnetars have been suggested [156].

4. Summary and conclusion

We have studied the medium modifications of magnetic moments and transition magnetic moments of the octet, decuplet, low-lying charm, and low-lying bottom baryons with nonzero light quarks in symmetric nuclear matter using the quark–meson coupling model, which satisfies the constraint for the allowed maximum change (swelling) of the nucleon size in medium, derived from the y-scaling data analysis—and thus satisfies the allowed maximum enhancement of the nucleon magnetic moment at the nuclear matter saturation density. The model has been extended to treat the decuplet baryons. This is the first study to estimate the in-medium magnetic moments and transition magnetic moments of the low-lying charm and low-lying bottom baryons with nonzero light quarks. In the estimates we have assumed the

"1–2 quark order" for the charm and bottom baryon flavor–spin wave functions as practised for the octet baryon SU(6) wave functions, namely, quarks 1 and 2 are the closest in mass. The issue of a different quark order is a concern for the $\Xi_{c,b}$ baryons in the present study. The "1–2 quark order" is supported as the best quark ordering for flavor-degenerate baryons for the masses.

In addition, we have estimated using two sets of current quark mass values, Set I (Table 1) and Set II (Table 2). The features obtained for the medium modifications are generally similar for the two sets.

The estimates of the medium modification are made by calculating the in-medium to free space baryon magnetic moment ratios, to compensate for the known MIT bag deficiency in obtaining the magnitude of the free space octet baryon magnetic moments. In connection with this, we have given examples where many experiments directly measure ratios to extract meaningful physics quantities, such as the electromagnetic form factors of the free and bound proton—experimental data extracted at Jefferson Laboratory support the in-medium to free ratios predicted by the quark–meson coupling model, and the European Muon Collaboration effect. The observed maximum modifications for the (octet, decuplet, charm, bottom) baryon sectors are, for the (Σ^-, Ξ^{*0}, Σ_c^+, Σ_b^0) baryons respectively and the corresponding modifications, about (12%, 158%, 17%, 12%) [11%, 257%, 17%, 12%)] at normal nuclear matter density ($\rho_0 = 0.15\,\text{fm}^{-3}$), and about (23%, 215%, 32%, 24%) [(25%, 414%, 32%, 23%)] at $3\rho_0$ for Set I [Set II], where the large enhancement of the Ξ^{*0} is due to the very small magnitude in free space in Set I [Set II].

As for the medium modifications of the transition magnetic moments $\mu_{BB'}$ with $B = (\Sigma^0, \Sigma_c^+, \Sigma_b^0) \to B' = (\Lambda, \Lambda_c^+, \Lambda_b^0)$, the modifications at ρ_0 are about (9%, 9%, 10%) [(9%, 9%, 10%)], while at $3\rho_0$ they are about (15%, 15%, 17%) [(16%, 15%, 17%)] for Set I [Set II]. Concerning the possible ambiguities arising from the MIT bag model artifact, we have discussed the difference of the initial and final baryon bag radii in free space as well as in symmetric nuclear matter, based on the evidence observed for the violation of the Ademollo–Gato theorem in the weak-interaction vector charge calculation. Furthermore, we have studied the possible impact of the ambiguities on the estimated results based on the SU(3) (U(3)) symmetry relations as well as the Coleman–Glashow relations using the calculated results and the experimental data. It turned out that such ambiguities are not expected to affect the estimated ratios of this study, within the present status of the experimental precision.

The medium modifications of baryon magnetic moments that have been estimated by the ratios in this study may serve as new realistic inputs for studies of magnetar and neutron star structure, in particular for systems with high baryon density with nearly zero temperature and extremely strong magnetic fields.

For practical use, we have given the explicit density-dependent parametrizations for the vector potentials of the baryons and light-(u, d) quarks, as well as for the effective masses of the low-lying baryons treated in this study, and of the ω, ρ, K, K^*, η, η', D, D^*, B, and B^* mesons. The parametrizations given in this study may open wider applications and studies for the properties of the corresponding baryons and mesons in medium.

As extensions, we plan to include the meson cloud effects in medium, and also study the medium modifications of the weak-interaction axial charges of the octet, decuplet, low-lying charm, and low-lying bottom baryons with nonzero light quarks.

Acknowledgments

Funding

References

[1] G. Barucca et al., [PANDA], Eur. Phys. J. A **57**, 184 (2021).
[2] S. Chakrabarty, D. Bandyopadhyay, and S. Pal, Phys. Rev. Lett. **78**, 2898 (1997).
[3] L. B. Leinson and A. Perez, J. High Energy Phys. **09**, 020 (1998).
[4] A. Broderick, M. Prakash, and J. M. Lattimer, Astrophys. J. **537**, 351 (2000).
[5] C. Y. Cardall, M. Prakash, and J. M. Lattimer, Astrophys. J. **554**, 322 (2001).
[6] G. J. Mao, A. Iwamoto, and Z. X. Li, Chin. J. Astron. Astrophys. **3**, 359 (2003).
[7] G. J. Mao, V. N. Kondratyev, A. Iwamoto, Z. Li, X. Wu, W. Greiner, and I. N. Mikhailov, Chin. Phys. Lett. **20**, 1238 (2003).
[8] P. Yue and H. Shen, Phys. Rev. C **74**, 045807 (2006).
[9] M. Sinha and D. Bandyopadhyay, Phys. Rev. D **79**, 123001 (2009).
[10] P. Yue, F. Yang, and H. Shen, Phys. Rev. C **79**, 025803 (2009) [arXiv:0902.3699 [nucl-th]] [Search inSPIRE].
[11] C. Y. Ryu, K. S. Kim, and M. K. Cheoun, Phys. Rev. C **82**, 025804 (2010).
[12] M. Sinha, B. Mukhopadhyay, and A. Sedrakian, Nucl. Phys. A **898**, 43 (2013).
[13] A. Rabhi, P. K. Panda, and C. Providencia, Phys. Rev. C **84**, 035803 (2011).
[14] D. Pena Arteaga, M. Grasso, E. Khan, and P. Ring, Phys. Rev. C **84**, 045806 (2011).
[15] C. Y. Ryu, M. K. Cheoun, T. Kajino, T. Maruyama, and G. J. Mathews, Astropart. Phys. **38**, 25 (2012).
[16] T. Maruyama, N. Yasutake, M. K. Cheoun, J. Hidaka, T. Kajino, G. J. Mathews, and C. Y. Ryu, Phys. Rev. D **86**, 123003 (2012).
[17] R. C. R. de Lima, S. S. Avancini, and C. Providência, Phys. Rev. C **88**, 035804 (2013).
[18] C. Kettner, F. Weber, M. K. Weigel, and N. K. Glendenning, Phys. Rev. D **51**, 1440 (1995).
[19] J. C. Jiménez and E. S. Fraga, Phys. Rev. D **102**, 034015 (2020).
[20] N. K. Glendenning, Compact Stars: Nuclear Physics, Particle Physics and General Relativity, 2nd ed. (Springer, New York, 2000).
[21] K. Tsushima, Phys. Rev. D **99**, 014026 (2019).
[22] P. A. M. Guichon, Phys. Lett. B **200**, 235 (1988).
[23] Y. Chen, H. Guo, and Y. Liu, Phys. Rev. C **75**, 035806 (2007).
[24] Y. Chen, Y. Yuan, and Y. Liu, Phys. Rev. C **79**, 055802 (2009).
[25] E. E. Kolomeitsev, K. A. Maslov, and D. N. Voskresensky, Nucl. Phys. A **961**, 106 (2017).
[26] T. Reichert, P. Hillmann, A. Limphirat, C. Herold, and M. Bleicher, J. Phys. G **46**, 105107 (2019).
[27] T. Reichert, P. Hillmann, and M. Bleicher, Nucl. Phys. A **1007**, 122058 (2021).
[28] J. J. Li and A. Sedrakian, Astrophys. J. Lett. **874**, L22 (2019).
[29] T. F. Motta, A. W. Thomas, and P. A. M. Guichon, Phys. Lett. B **802**, 135266 (2020).
[30] J. J. Li, A. Sedrakian, and F. Weber, Phys. Lett. B **810**, 135812 (2020).
[31] V. B. Thapa, M. Sinha, J. J. Li, and A. Sedrakian, Phys. Rev. D **103**, 063004 (2021).
[32] V. Dexheimer, K. D. Marquez, and D. P. Menezes, Eur. Phys. J. A **57**, 216 (2021).
[33] P. A. M. Guichon, K. Saito, E. N. Rodionov, and A. W. Thomas, Nucl. Phys. A **601**, 349 (1996).
[34] K. Saito, K. Tsushima, and A. W. Thomas, Nucl. Phys. A **609**, 339 (1996).
[35] K. Saito, K. Tsushima, and A. W. Thomas, Phys. Rev. C **55**, 2637 (1997).

[36] J. R. Stone, P. A. M. Guichon, P. G. Reinhard, and A. W. Thomas, Phys. Rev. Lett. **116**, 092501 (2016).

[37] K. Tsushima, K. Saito, and A. W. Thomas, Phys. Lett. B **411**, 9 (1997); 421, 413 (1998) [erratum].

[38] K. Tsushima, K. Saito, J. Haidenbauer, and A. W. Thomas, Nucl. Phys. A **630**, 691 (1998).

[39] P. A. M. Guichon, A. W. Thomas, and K. Tsushima, Nucl. Phys. A **814**, 66 (2008).

[40] K. Tsushima and F. C. Khanna, Phys. Rev. C **67**, 015211 (2003).

[41] K. Tsushima and F. C. Khanna, Prog. Theor. Phys. Suppl. **149**, 160 (2003).

[42] K. Tsushima and F. C. Khanna, J. Phys. G **30**, 1765 (2004).

[43] K. Saito, K. Tsushima, and A. W. Thomas, Phys. Rev. C **56**, 566 (1997).

[44] K. Tsushima, K. Saito, A. W. Thomas, and S. V. Wright, Phys. Lett. B **429**, 239 (1998); 436, 453 (1998) [erratum].

[45] K. Tsushima, D. H. Lu, A. W. Thomas, and K. Saito, Phys. Lett. B **443**, 26 (1998).

[46] K. Tsushima, Nucl. Phys. A **670**, 198 (2000).

[47] K. Tsushima, D. H. Lu, A. W. Thomas, K. Saito, and R. H. Landau, Phys. Rev. C **59**, 2824 (1999).

[48] A. Sibirtsev, K. Tsushima, K. Saito, and A. W. Thomas, Phys. Lett. B **484**, 23 (2000).

[49] K. Tsushima and F. C. Khanna, Phys. Lett. B **552**, 138 (2003).

[50] A. Sibirtsev, K. Tsushima, and A. W. Thomas, Eur. Phys. J. A **6**, 351 (1999).

[51] R. Shyam, K. Tsushima, and A. W. Thomas, Phys. Lett. B **676**, 51 (2009).

[52] K. Tsushima, P. A. M. Guichon, R. Shyam, and A. W. Thomas, Int. J. Mod. Phys. E **19**, 2546 (2010).

[53] R. Shyam, K. Tsushima, and A. W. Thomas, Nucl. Phys. A **881**, 255 (2012).

[54] R. Chatterjee, R. Shyam, K. Tsushima, and A. W. Thomas, Nucl. Phys. A **913**, 116 (2013).

[55] K. Tsushima, R. Shyam, and A. W. Thomas, Few Body Syst. **54**, 1271 (2013).

[56] R. Shyam and K. Tsushima, Phys. Rev. D **94**, 074041 (2016).

[57] R. Shyam and K. Tsushima, Phys. Lett. B **770**, 236 (2017).

[58] R. Shyam and K. Tsushima, Few Body Syst. **59**, 18 (2018).

[59] J. Rikovska-Stone, P. A. M. Guichon, H. H. Matevosyan, and A. W. Thomas, Nucl. Phys. A **792**, 341 (2007).

[60] T. Katayama, T. Miyatsu, and K. Saito, Astrophys. J. Suppl. **203**, 22 (2012).

[61] T. Miyatsu, T. Katayama, and K. Saito, Phys. Lett. B **709**, 242 (2012).

[62] D. L. Whittenbury, J. D. Carroll, A. W. Thomas, K. Tsushima, and J. R. Stone, Phys. Rev. C **89**, 065801 (2014).

[63] A. W. Thomas, D. L. Whittenbury, J. D. Carroll, K. Tsushimam, and J. R. Stone, EPJ Web Conf. **63**, 03004 (2013).

[64] K. Saito, K. Tsushima, and A. W. Thomas, Prog. Part. Nucl. Phys. **58**, 1 (2007).

[65] G. Krein, A. W. Thomas, and K. Tsushima, Prog. Part. Nucl. Phys. **100**, 161 (2018).

[66] P. A. M. Guichon, J. R. Stone, and A. W. Thomas, Prog. Part. Nucl. Phys. **100**, 262 (2018).

[67] R. Shyam and K. Tsushima, arXiv:1901.06090 [nucl-th] [Search inSPIRE].

[68] M. Yoshimoto et al. Prog. Theor. Exp. Phys. **2021**, 7 (2021).

[69] S. Nagai, T. Miyatsu, K. Saito, and K. Tsushima, Phys. Lett. B **666**, 239 (2008).

[70] S. Choi, T. Miyatsu, Y. Kwon, K. Kim, M. K. Cheoun, and K. Saito, Phys. Rev. C **104**, 014322 (2021).

[71] P. Gubler and K. Ohtani, Phys. Rev. D **90**, 094002 (2014).

[72] P. Gubler and D. Satow, Prog. Part. Nucl. Phys. **106**, 1 (2019).

[73] K. Tsushima, T. Maruyama, and A. Faessler, Nucl. Phys. A **535**, 497 (1991).

[74] T. Maruyama, K. Tsushima, and A. Faessler, Nucl. Phys. A **537**, 303 (1992).

[75] M. A. Shifman, A. I. Vainshtein, and V. I. Zakharov, Nucl. Phys. B **147**, 385 (1979).

[76] D. Antonov and J. E. F. T. Ribeiro, Eur. Phys. J. C **72**, 2179 (2012).

[77] T. D. Cohen, R. J. Furnstahl, and D. K. Griegel, Phys. Rev. C **45**, 1881 (1992).

[78] A. A. Tyapkin, Sov. J. Nucl. Phys. **22**, 89 (1976).

[79] C. B. Dover and S. H. Kahana, Phys. Rev. Lett. **39**, 1506 (1977).

[80] B. F. Gibson, C. B. Dover, Bhamati, and D. R. Lehman, Phys. Rev. C **27**, 2085 (1982).

[81] H. Bando and M. Bando, Phys. Lett. B **109**, 164 (1982).

[82] H. Bando and S. Nagata, Prog. Theor. Phys. **69**, 557 (1983).

[83] T. Bressani and F. Iazzi, Nuovo Cim. A **102**, 1597 (1989).

[84] S. A. Buyatov, V. V. Lyukov, N. I. Strakov, and V. A. Tsarev, Nuovo Cim. A **104**, 1361 (1991).
[85] Y. H. Tan and P. Z. Ning, Europhys. Lett. **67**, 355 (2004).
[86] Z. G. Wang, Eur. Phys. J. C **71**, 1816 (2011).
[87] Z. G. Wang, Phys. Rev. C **85**, 045204 (2012).
[88] Z.-G. Wang, Eur. Phys. J. C **72**, 2099 (2012).
[89] S. Ghosh, S. K. Das, V. Greco, S. Sarkar, and J. e. Alam, Phys. Rev. D **90**, 054018 (2014).
[90] A. Hosaka, T. Hyodo, K. Sudoh, Y. Yamaguchi, and S. Yasui, Prog. Part. Nucl. Phys. **96**, 88 (2017).
[91] K. Azizi, N. Er, and H. Sundu, Nucl. Phys. A **960**, 147 (2017); 962, 122 (2017) [erratum].
[92] K. Azizi and N. Er, Nucl. Phys. A **970**, 422 (2018).
[93] N. Er and K. Azizi, Phys. Rev. D **99**, 074012 (2019).
[94] K. Azizi and N. Er, Phys. Rev. D **100**, 074004 (2019).
[95] K. Ohtani, K. j. Araki, and M. Oka, Phys. Rev. C **96**, 055208 (2017).
[96] T. F. Caramés, C. E. Fontoura, G. Krein, J. Vijande, and A. Valcarce, Phys. Rev. D **98**, 114019 (2018).
[97] S. Yasui, Phys. Rev. C **100**, 065201 (2019).
[98] I. Vidaña, A. Ramos, and C. E. Jimenez-Tejero, Phys. Rev. C **99**, 045208 (2019).
[99] M. Abu-Shady and A. N. Ikot, Eur. Phys. J. Plus **135**, 406 (2020).
[100] C. Y. Ryu, C. H. Hyun, T.-S. Park, and S. W. Hong, Phys. Lett. B **674**, 122 (2009).
[101] G. Ramalho, K. Tsushima, and A. W. Thomas, J. Phys. G **40**, 015102 (2013).
[102] H. Singh, A. Kumar, and H. Dahiya, Eur. Phys. J. Plus **134**, 128 (2019).
[103] H. Singh, A. Kumar, and H. Dahiya, Eur. Phys. J. Plus **135**, 422 (2020).
[104] D. B. Lichtenberg, Phys. Rev. D **15**, 345 (1977).
[105] R. J. Johnson and M. Shah-Jahan, Phys. Rev. D **15**, 1400 (1977).
[106] J. Franklin, D. B. Lichtenberg, W. Namgung, and D. Carydas, Phys. Rev. D **24**, 2910 (1981).
[107] S. K. Bose and L. P. Singh, Phys. Rev. D **22**, 773 (1980).
[108] A. Bernotas and V. Simonis, arXiv:1209.2900 [hep-ph] [Search inSPIRE].
[109] A. Bernotas and V. Simonis, Phys. Rev. D **87**, 074016 (2013).
[110] V. Simonis, arXiv:1803.01809 [hep-ph] [Search inSPIRE].
[111] T. M. Aliev, T. Barakat, and M. Savci, Phys. Rev. D **91**, 116008 (2015).
[112] T. M. Aliev, K. Azizi, T. Barakat, and M. Savcı, Phys. Rev. D **92**, 036004 (2015).
[113] A. Faessler, T. Gutsche, M. A. Ivanov, J. G. Korner, V. E. Lyubovitskij, D. Nicmorus, and K. Pumsa-ard, Phys. Rev. D **73**, 094013 (2006).
[114] B. Patel, A. K. Rai, and P. C. Vinodkumar, J. Phys. G **35**, 065001 (2008).
[115] N. Barik and M. Das, Phys. Rev. D **28**, 2823 (1983)
[116] S. N. Jena and D. P. Rath, Phys. Rev. D **34**, 196 (1986).
[117] I. Sick, Phys. Lett. B **157**, 13 (1985).
[118] I. Sick, Medium effects on nucleon size, in Weak and Electromagnetic Interactions in Nuclei, ed. H. V. Klapdor Klapdor (Springer, Berlin, 1986), p. 415.
[119] R. D. McKeown, Phys. Rev. Lett. **56**, 1452 (1986).
[120] J. Morgenstern and Z. E. Meziani, Phys. Lett. B **515**, 269 (2001).
[121] D. H. Lu, A. W. Thomas, K. Tsushima, A. G. Williams, and K. Saito, Phys. Lett. B **417**, 217 (1998).
[122] D. H. Lu, K. Tsushima, A. W. Thomas, A. G. Williams, and K. Saito, Phys. Rev. C **60**, 068201 (1999).
[123] M. K. Jones et al. [Jefferson Lab Hall A], Phys. Rev. Lett. **84**, 1398 (2000).
[124] O. Gayou et al. [Jefferson Lab Hall A], Phys. Rev. Lett. **88**, 092301 (2002).
[125] S. Strauch et al. [Jefferson Lab E93-049], Phys. Rev. Lett. **91**, 052301 (2003).
[126] S. Dieterich et al., Phys. Lett. B **500**, 47 (2001).
[127] M. Paolone et al., Phys. Rev. Lett. **105**, 072001 (2010).
[128] S. Malov et al., Phys. Rev. C **62**, 057302 (2000).
[129] A. Bodek et al., Phys. Rev. Lett. **50**, 1431 (1983).
[130] J. Seely et al., Phys. Rev. Lett. **103**, 202301 (2009).
[131] J. J. Auberto et al. [The European Muon Collaboration], Phys. Lett. B **123**, 275 (1983).
[132] Q. X. Yu, R. Pavao, V. R. Debastiani, and E. Oset, Eur. Phys. J. C **79**, 167 (2019).
[133] G. Krein, A. W. Thomas, and K. Tsushima, Nucl. Phys. A **650**, 313 (1999).

[134] J. D. Walecka, Ann. Phys. **83**, 491 (1974).
[135] B. D. Serot and J. D. Walecka, Adv. Nucl. Phys. **16**, 1 (1986).
[136] A. Chodos, R. L. Jaffe, K. Johnson, C. B. Thorn, and V. F. Weisskopf, Phys. Rev. D **9**, 3471 (1974).
[137] P. A. M. Guichon, H. H. Matevosyan, N. Sandulescu, and A. W. Thomas, Nucl. Phys. A **772**, 1 (2006).
[138] M. Dutra, O. Lourenco, J. S. Sa Martins, A. Delfino, J. R. Stone, and P. D. Stevenson, Phys. Rev. C **85**, 035201 (2012).
[139] P. A. Zyla et al. [Particle Data Group], Prog. Theor. Exp. Phys. **2020**, 083C01 (2020).
[140] P. Kienle and T. Yamazaki, Prog. Part. Nucl. Phys. **52**, 85 (2004).
[141] U. Vogl and W. Weise, Prog. Part. Nucl. Phys. **27**, 195 (1991).
[142] U. G. Meissner, J. A. Oller, and A. Wirzba, Ann. Phys. **297**, 27 (2002).
[143] M. Ademollo and R. Gatto, Phys. Rev. Lett. **13**, 264 (1964).
[144] P. A. M. Guichon and A. W. Thomas, Phys. Lett. B **773**, 332 (2017).
[145] D. B. Leinweber, R. M. Woloshyn, and T. Draper, Phys. Rev. D **43**, 1659 (1991).
[146] D. B. Leinweber, T. Draper, and R. M. Woloshyn, Phys. Rev. D **46**, 3067 (1992).
[147] F. X. Lee, R. Kelly, L. Zhou, and W. Wilcox, Phys. Lett. B **627**, 71 (2005).
[148] S. Okubo, Prog. Theor. Phys. **27**, 949 (1962).
[149] Y. Ne'eman, Nucl. Phys. **26**, 222 (1961).
[150] M. Gell-Mann, Phys. Rev. **125**, 1067 (1962).
[151] T. A. DeGrand, R. L. Jaffe, K. Johnson, and J. E. Kiskis, Phys. Rev. D **12**, 2060 (1975).
[152] E. Allen, Phys. Lett. B **57**, 263 (1975).
[153] T. Yamaguchi, K. Tsushima, Y. Kohyama, and K. Kubodera, Nucl. Phys. A **500**, 429 (1989).
[154] S. R. Coleman and S. L. Glashow, Phys. Rev. Lett. **6**, 423 (1961).
[155] G. M. Hossain and S. Mandal, arXiv:2005.08783 [gr-qc] [Search inSPIRE].
[156] J. A. Carpio, K. Murase, M. H. Reno, and A. Stasto, arXiv:2007.07945 [astro-ph.HE] [Search in SPIRE].